CFD ANALYSIS ON FORCED CONVECTION COOLING OF ELECTRONIC CHIPS

A THESIS SUBMITTED IN PARTIAL FULFILMENT
OF THE REQUIREMENTS FOR THE DEGREE OF

Master of Technology (Research)

in

Mechanical Engineering

by

SHAKUNTALA OJHA

Department of Mechanical Engineering
National Institute of Technology
Rourkela

2009

National Institute of Technology
Rourkela

CERTIFICATE

This is to certify that thesis entitled, "**CFD ANALYSIS ON FORCED CONVECTION COOLING OF ELECTRONIC CHIPS**" submitted by **Ms. Shakuntala Ojha** in partial fulfillment of the requirements for the award of **Master of Technology Degree (Research)** in Mechanical Engineering with specialization in "**Thermal Engineering**" at National Institute of Technology, Rourkela (Deemed University) is an authentic work carried out by her under our supervision and guidance.

To the best of our knowledge, the matter embodied in this thesis has not been submitted to any other university/ institute for award of any Degree or Diploma.

Co-guide **Guide**

Prof. R.K. Sahoo **Prof. A.K. Satapathy**

Dept. of Mechanical Engineering Dept. of Mechanical Engineering

National Institute of Technology National Institute of Technology

ACKNOWLEDGEMENT

It is with a feeling of great pleasure that I would like to express my most sincere heartfelt gratitude to **Prof. A.K. Satapathy, Dept. of Mechanical Engineering, NIT, Rourkela** for suggesting the topic for my thesis report and for his ready and able guidance throughout the course of my preparing the report. I am greatly indebted to him for his constructive suggestions and criticism from time to time during the course of progress of my work.

I express my sincere thanks to **Prof. R.K. Sahoo, HOD, Department of Mechanical Engineering, NIT, Rourkela** for providing me the necessary facilities in the department.

I wish to express my sincere gratitude to **Prof. R.K. Mallik, Dept. of Mechanical Engineering, UCE, Burla** for his continuous encouragement, helping me in understanding the problem and technical know-how support for modeling in FLUENT during perusal of this thesis desertion.

I am also thankful to all my friends and the staff members of the department of Mechanical Engineering and to all my well wishers for their inspiration and help.

Finally, I express my deepest gratitude to my parents for their continuous encouragement, understanding and support.

Shakuntala Ojha

Date: - **Roll No: - 60703001**

National Institute of Technology

Rourkela-769008, Orissa, India

ABSTRACT

For more than a decade, investigations have been conducted to better understand the fluid flow and heat transfer characteristics in silicon-based microchannel heat sinks designed for applications in electronic cooling. These non-circular channels and silicon based microchannel heat sinks combine the attributes of high material compatibility, high surface area per unit volume ratios and large potential heat transfer performance with highly sophisticated and economic fabrication process. These advantages make these silicon based microchannel heat sinks extremely attractive for a wide variety of commercial applications.

The present work addresses electronic chips cooling with forced convection of water in silicon based single microchannel heat sinks by the help of a commercial CFD software FLUENT. The computational domain is discretized with non-uniform grids on the flow face but uniform grid along the flow. For single microchannel, the grid is generated by implementing Gambit software, which is incorporated with Cooper method for 3-dimensional grid generation. The pressure, velocity and temperature contours at inlet and outlet are presented along with the variation of these fields in flow direction for visual comparisons. The output of the single microchannel is in good agreement with the available results for silicon substrate. The Nusselt number variation along the flow direction is presented and compared for three different flow rates. The convection heat transfer co-efficient is also presented for above three cases. During simulation of the aforementioned cases, Semi-Implicit Method for Pressure Linked Equations (SIMPLE) with second order upwind scheme is implemented for laminar fully-developed flow. The continuity, momentum and energy equations are solved in a segregated manner because of its accuracy. As the fluid flows in a microchannel, the laminar flow is considered during simulation along with the energy equation. The single microchannel solution is converged quickly with minimum number of iterations. The post processing of the output results are carried out by Excel.

Three different pressure drops are taken into consideration during simulation. As the pressure difference is directly related to the pumping power, the optimization of power consumption can be entertained by this simulation. The maximum pressure difference can be taken for more heat

flux condition imposed on the boundary and also to suppress the temperature rise in the sink. For instance, for the simulation of a single microchannel, the temperature rise of the heat sink for 10 kPa, 20 kPa, 35 kPa, 50 kPa and 65 kPa are found to 62 ^{o}C, 56 ^{o}C, 46 ^{o}C, 36 ^{o}C and 26 ^{o}C respectively for silicon heat sink when the heat flux is in the order of 9×10^{5} W/m^{2}. Eventually, it is quite pertinent to suppress the temperature rise of water in the microchannel above the boiling point of water. The post processing results of single microchannel is in good agreement with the available results. The velocity, temperature and pressure difference profiles at inlet, outlet and along the channel are presented after simulation of the aforementioned conditions.

Table of Contents

List of Figures

List of Tables

Nomenclature

English Symbols

A	area of cross-section of microchannel
A_w	area of cross-section of substrate bottom wall
c_p	specific heat
D_h	hydraulic diameter
f	friction factor
H	height of the microchannel heat sink
h	channel depth, convective heat transfer coefficient
k	thermal conductivity
L	length of microchannel, characteristics length
P	pressure
q''	heat flux
T	temperature
W	width of heat sink
w	width of channel, z-component velocity
u,v,w	velocity components
x,y,z	cartesian coordinates

Subscripts

avg	averaged value
b	bottom thickness of heat sink
f	fluid
h	hydraulic
in	at inlet of channel
out	at outlet of channel
s	solid
t	top thickness of heat sink
w	substrate wall

Greek symbols

v	kinematic viscosity
μ	dynamic viscosity
α	thermal diffusivity
ρ	density
Γ	periphery of inner wall of channel
λ	mean free path

Non-Dimensional groups

Re	Reynolds number
Nu	Nusselt number
K_n	Knudsen number

Abbreviations

VLSI	Very Large Scale Integration
MEMS	Micro-Electro Mechanical Systems
ENIAC	Electrical Numerical Integrator and Computer
SSI	Small scale integration
MSI	Medium scale integration
LSI	Large scale integration
MMC	Manifold microchannel
CGR	Cumulative growth rate
CATE	Computer aided thermal engineering
CDU	Coolant distribution unit
PCB	Component-printed circuit board

CHAPTER 1

Introduction

- ***General***
- ***New Thermal Design Requirements***
- ***Cooling Methods Used in Industry***
- ***Heat Sink***
- ***Microchannel Heat Sink***
- ***Objective of the Work***
- ***Organization of the Thesis***

1.1 General

Recently the developments concerned with the VLSI technology and MEMS demand the fabrication of electronic chips on a single silicon wafers for which microchannels are to be imbedded with these silicon based micro systems. Hence, understanding the heat and fluid flow phenomena through the microchannels are the major thrust area of electronic packaging engineers. The thermal energy developed during the relentless operation of electronics chips is to be dissipated by incorporating efficient heat sinks on the chips. It has been observed that the chip failures are caused primarily due to the temperature rise in the circuits because of accumulation of heat. Hence, microchannel embedded chips are the possible solution to ultra-compact electronics gadgets.

Since the development of the first electronic digital computers in the 1940s, the effective removal of heat has played a key role in ensuring the reliable operation of successive generations of computers. The ENIAC, has been described as a ‘‘30 ton, boxcar-sized machine requiring an array of industrial cooling fans to remove the 140 KW dissipated from its 18,000 vacuum tubes’’. As with ENIAC, all early computers used vacuum-tube electronics and were cooled with forced air. As a replacement for vacuum tubes, the miniature transistor generated less heat, was much more reliable, and promised lower production costs. For a while it was thought that the use of transistors would greatly reduce if not totally eliminate cooling concerns. This thought was short-lived as packaging engineers worked to improve computer speed and storage capacity by packaging more and more transistors on printed circuit boards, and then on ceramic substrates.

The trend toward higher packaging densities dramatically gained momentum with the invention of the integrated circuit. During the 1960s SSI and then MSI led from one device per chip to hundreds of devices per chip. The trend continued through the 1970s with the development of LSI technologies offering hundreds to thousands of devices per chip, and then through the 1980s with the development of VLSI technologies offering thousands to tens of thousands of devices per chip (Fig. 1.1). In many instances the trend toward higher circuit

density has been accompanied by increased power dissipation per circuit to provide reductions in circuit delay (i.e., increased speed). The need to further increase packaging density and to reduce signal delay between communicating circuits led to the development of multi chip modules began in the late 1970s and is continuing to this day. Fig. 1.2 and Fig. 1.3 represent the chip heat flux and module heat flux. It can be seen that the chip heat flux increases at a CGR of 7 % per year, and heat flux associated with bipolar circuit technologies steadily increased from the very beginning and really took off in the 1980s. There was a brief respite with the transition to CMOS circuit technologies in the 1990s; but the demand for increased packaging density and performance reasserted itself and heat flux is again increasing at a challenging rate.

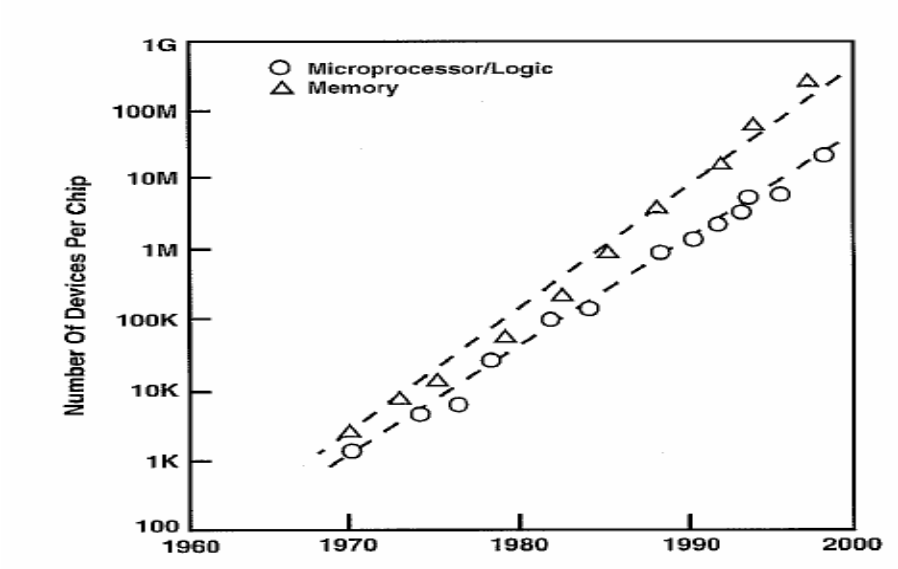

Fig. 1.1. Increase in circuit complexity.

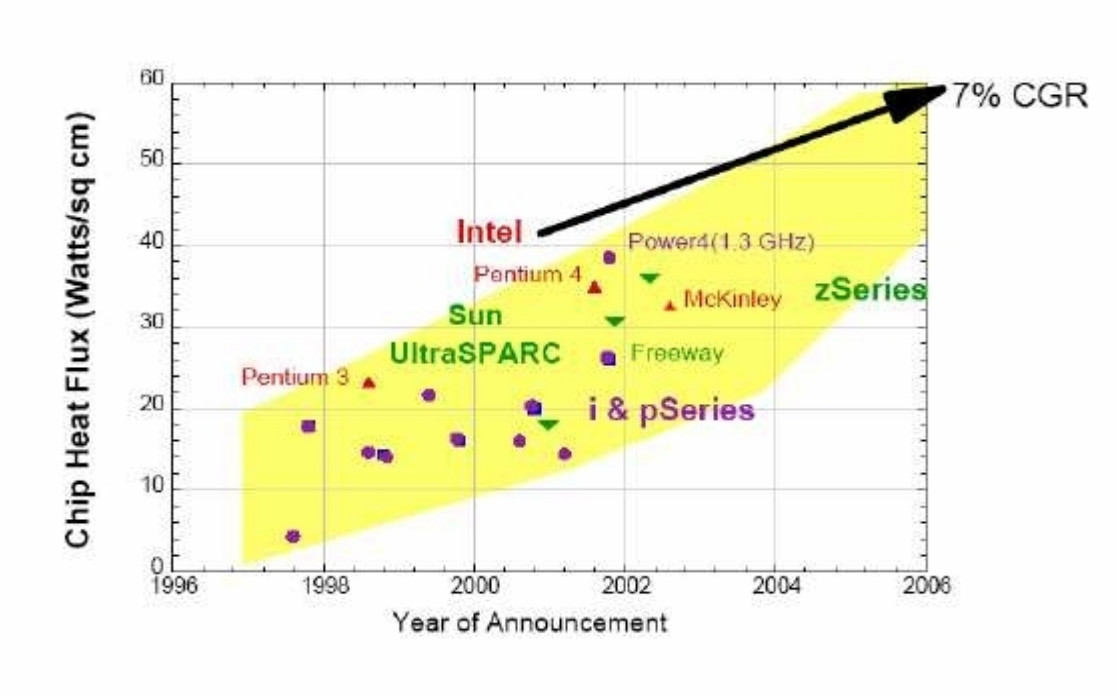

Fig. 1.2. The chronological evolution of chip level heat flux.

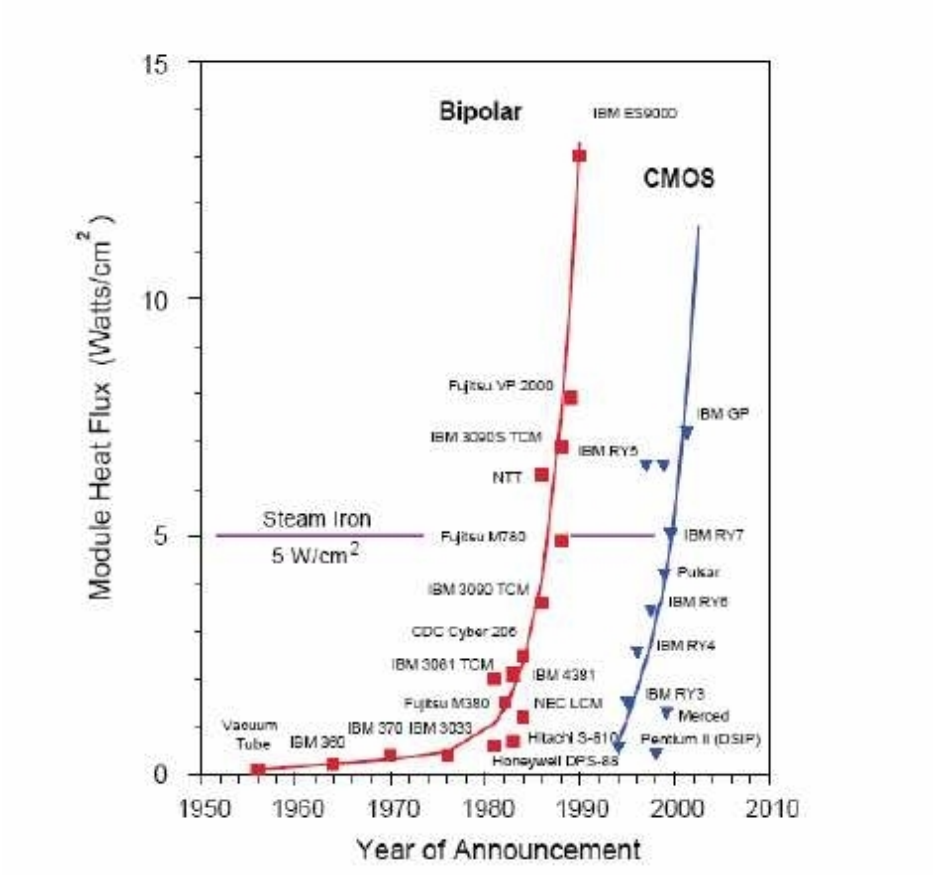

Fig. 1.3. The chronological evolution of module level heat Flux in mainframe computers.

It has been found that for every 2 ºC temperature rise, the reliability of a silicon chip will be decreased by about 10 %. The major cause of an electronic chip failure is due to temperature rise (55%) as against other factors which accounts 20 % vibration, 19 % humidity and 6 % dust (Fig. 1.4). So it's a great challenge for the packaging engineers to remove the heat from the electronics chips very effectively.

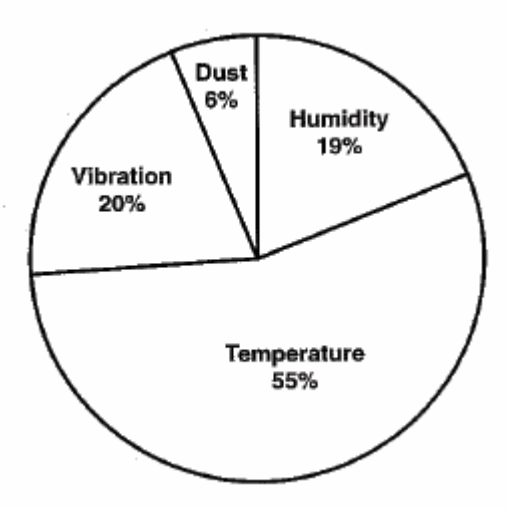

Fig. 1.4. Major causes of electronics failure.

Throughout the past 50 years, cooling and thermal management have played a key role in accommodating the increase in power while maintaining component temperatures at satisfactory levels to satisfy performance and reliability objectives. Thermal management will play a pivotal role in the coming decade for all types of electronics products. Increased heat fluxes at all levels of packaging from chip to system to facility pose a major cooling challenge. To meet the challenge, significant cooling technology enhancements will be needed in each of the following areas:-

Thermal interfaces, Heat spreading, Air cooling, Indirect and direct water cooling, Immersion cooling, Refrigeration cooling, Thermoelectric cooling and Data center cooling.

So the thermal design requirements to meet the growing demands are as follows, it is here the Traditional Thermal Design Requirements are explained and categorized as follows:-

Design for Performance, Design for Reliability, Design for Serviceability, Design for Extensibility, Design for minimal cost and Design on minimal Impact on User.

1.2 New Thermal Design Requirements

- Design for improved cool ability at the package level via optimized internal thermal conduction paths.
- Design for direct air cooling at the product level via enhanced convection process over the packages.
- Design for special cooling needs at the module level via spot cooling devices attached to the packages.
- Design for low temperature applications-Sub ambient to cryogenic.
- Design for low cost via CATE and improved manufacturability.

1.3 Cooling Methods Used in Industry

Here are the various types of methods used in electronics (Computer) industry to cool Modules, Systems, and Data centers.

1.3.1 Module Level Cooling

Processor module cooling is typically characterized in two ways: cooling internal and external to the module package and applies to both single and multi chip modules. Fig. 1.5 illustrates the distinction between the two cooling regimes in the context of a single-chip module.

1.3.1.1 Internal Module Cooling

The primary mode of heat transfer internal to the module is by conduction. The internal thermal resistance is therefore dictated by the module's physical construction and material properties. The objective is to effectively transfer the heat from the electronics circuits to an outer surface of the module where the heat will be removed by external means which will be discussed in the following section.

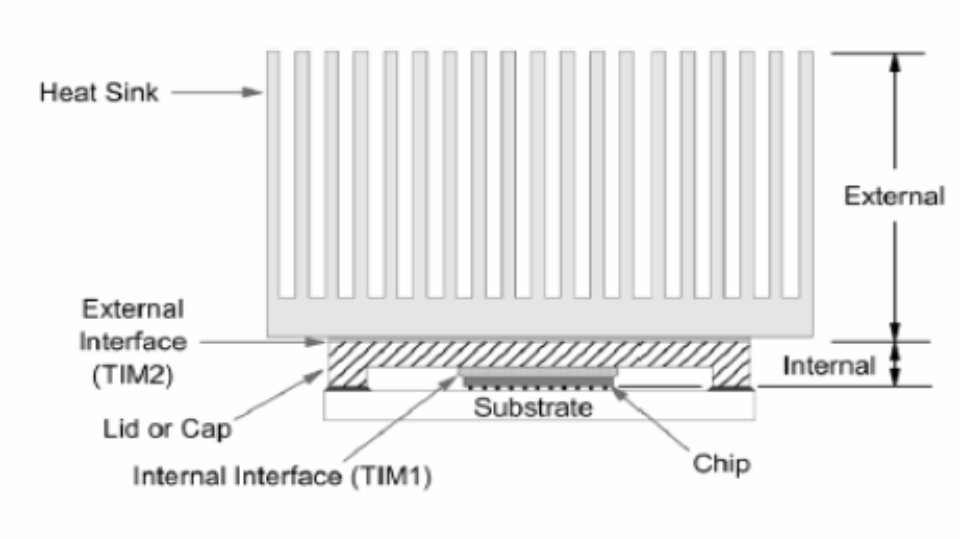

Fig. 1.5. Cross-section of a typical module denoting internal cooling region and external cooling region.

1.3.1.2 External Module Cooling

Cooling external to the module serves as the primary means to effectively transfer the heat generated within the module to the system environment. This is accomplished primarily by attaching a heat sink to the module. Traditionally, and preferably, the system environment of choice has been air because of its ease of implementation, low cost, and transparency to the end user or customer.

1.3.1.3 Immersion Cooling

Immersion cooling has been of interest as a possible method to cool high heat flux components for many years. Unlike the water-cooled cold plate approaches, which utilize physical walls to separate the coolant from the chips, immersion cooling brings the coolant in direct physical contact with the chips. Direct liquid immersion cooling offers a high heat transfer coefficient which reduces the temperature rise of the heated chip surface above the liquid coolant temperature. The magnitude of the heat transfer coefficient depends upon the thermo-physical properties of the coolant and the mode of convective heat transfer employed. The modes of heat transfer associated with liquid immersion cooling are generally classified as natural convection, forced convection, and boiling. Forced convection includes liquid jet impingement in the single

phase regime and boiling (including pool boiling, flow boiling, and spray cooling) in the two-phase regime.

1.3.2 System Level Cooling

Cooling systems for computers may be categorized as air-cooled, hybrid-cooled, liquid-cooled, or refrigeration-cooled. An air-cooled system is one in which air, usually in the forced convection mode, is used to directly cool and carry heat away from arrays of electronic modules and packages. In some systems air-cooling alone may not be adequate due to heating of the cooling air as it passes through the machine. In such cases a hybrid-cooling design may be employed, with air used to cool the electronic packages and water-cooled heat exchangers used to cool the air. For even higher power packages it may be necessary to employ indirect liquid cooling. This is usually done utilizing water-cooled cold plates on which heat dissipating components are mounted or which may be mounted to modules containing integrated circuit chips. Ultimately, direct liquid immersion cooling may be employed to accommodate high heat fluxes and a high system heat load.

1.3.2.1 Air Cooling

Although liquid forced convection and boiling offer the highest heat transfer rates, air cooling be the most widely used technique for heat rejection. The principal advantages of cooling with air are its ready availability and ease of application. All computers were cooled solely by forced air. Air moving devices took in room and provided a serial flow of air over columns of boards carrying printed circuit cards with single chip modules. In many cases air moving devices at either the bottom or top of a column of boards provided sufficient cooling air flow. A push-pull airflow arrangement with air moving devices at both the bottom and top of the column of boards was used for those cases requiring higher pressure drop capability.

Forced air-cooled systems may be further subdivided into serial and parallel flow systems. In a serial flow system the same air stream passes over successive rows of modules or boards, so that each row is cooled by air that has been preheated by the previous row. Depending on the power dissipated and the air flow rate, serial air flow can result in a substantial air temperature rise across the machine. The rise in cooling air temperature is directly reflected in increased circuit

operating temperatures. This effect may be reduced by increasing the air flow rate. Of course to do this requires larger blowers to provide the higher flow rate and overcome the increase in air flow pressure drop. Parallel air flow systems have been used to reduce the temperature rise in the cooling air. In systems of this type, the printed circuit boards or modules are all supplied air in parallel. Since each board or module is delivered its own fresh supply of cooling air.

1.3.2.2 Hybrid Air-Water Cooling

An air-to-liquid hybrid cooling system offers a method to manage cooling air temperature in a system without resorting to a parallel configuration and higher air flow rates. In a system of this type, a water-cooled heat exchanger is placed in the heated air stream to extract heat and reduce the air temperature. The cooling system incorporated an air-to-water finned tube heat exchanger between each successive row of circuit boards. The modules on the boards were still cooled by forced convection with air, however; the heated air exiting a board passed through an air-to-water heat exchanger before passing over the next board. Approximately 50% of the heat transferred to air in the board columns was transferred to the cooling water. Ultimately air-to-liquid hybrid cooling offers the potential for a sealed, recirculation and closed-cycle air-cooling system with total heat rejection of the heat load absorbed by the air to chilled water. Sealing the system offers additional advantages. It allows the use of more powerful blowers to deliver higher air flow rates with little or no impact on acoustics. In addition, the potential for electromagnetic emissions from air inlet/outlet openings in the computer frame is eliminated. Another variant of the hybrid cooling system is the liquid-to-air cooling system. In this system liquid is circulated in a sealed loop through a cold plate attached to an electronic module dissipating heat. The heat is then transported via the liquid stream to an air-cooled heat exchanger where it is rejected to ambient air. This scheme provides the performance advantages of indirect liquid cooling at the module level while retaining the advantages of air cooling at the system or box level.

1.3.2.3 Liquid-Cooling Systems

Either the air-to-water heat exchangers in a hybrid air-water-cooled system or the water-cooled cold plates in a conduction-cooled system rely upon a controlled source of water in terms of pressure, flow rate, temperature. In order to insure the physical integrity, performance, and long-term reliability of the cooling system, water is usually not run directly through the water-carrying

components in electronic frames. This is because of the great variability that can exist in the quality of water available at computer installations throughout the world. Instead a pumping and heat exchange unit, sometimes called CDU is used to control and distribute system cooling water to computer electronics frames. The primary closed loop (i.e., system) is used to circulate cooling water to and from the electronics frames. The system heat load is transferred to the secondary loop (i.e., customer water) via a water-to-water heat exchanger in the CDU. Within an electronics frame a combination of parallel-series flow networks is used to distribute water flow to individual cold plates and heat exchangers. Water flow in the primary loop is provided at a fixed flow rate by a single operating pump, with a stand-by pump to provide uninterrupted operation if the operating pumps fails. The temperature of the water in the primary loop is controlled by using a mixing valve to regulate the fraction of the flow allowed to pass through the water-to-water heat exchanger and forcing the remainder to bypass the heat exchanger. A CDU is also required for direct immersion cooling systems. In addition, because of the relatively high vapor pressure of the coolants suitable for direct immersion applications (e.g., fluorocarbons), the cooling system must be both “vapor-tight” and “liquid-tight” to ensure against any loss of the relatively expensive coolant.

1.3.2.4 Refrigeration Cooled Systems

The potential for enhancement of computer performance by operating at lower temperatures was recognized as long ago as the late 1960s and mid 1970s. Some of the earliest studies focused on Josephson devices operating at liquid helium temperatures (4K). The focus then shifted to CMOS devices operating near liquid nitrogen temperatures (77 K). A number of researchers have identified the electrical advantages of operating electronics all the way down to liquid nitrogen temperatures (77 K). The advantages are:

- Increased average carrier drift velocities (even at high fields);
- Steeper sub-threshold slope, plus reduced sub-threshold currents (channel leakages) which provide higher noise margins;
- Higher transconductance;
- Well-defined threshold voltage behavior;
- No degradation of geometry effects;
- Enhanced electrical line conductivity;

1.3.3 Data Center Thermal Management

Due to technology compaction, the information technology industry has seen a large decrease in the floor space required to achieve a constant quantity of computing and storage capability. However, the energy efficiency of the equipment has not dropped at the same rate. This has resulted in a significant increase in power density and heat dissipation within the footprint of computer and telecommunications hardware. The heat dissipated in these systems is exhausted to the room and the room has to be maintained at acceptable temperatures for reliable operation of the equipment. Cooling computer and telecommunications equipment rooms is becoming a major challenge. The increasing heat load of data-com equipment has been documented by a thermal management consortium of 17 companies and published in collaboration with the Uptime Institute as shown in Fig. 1.6.

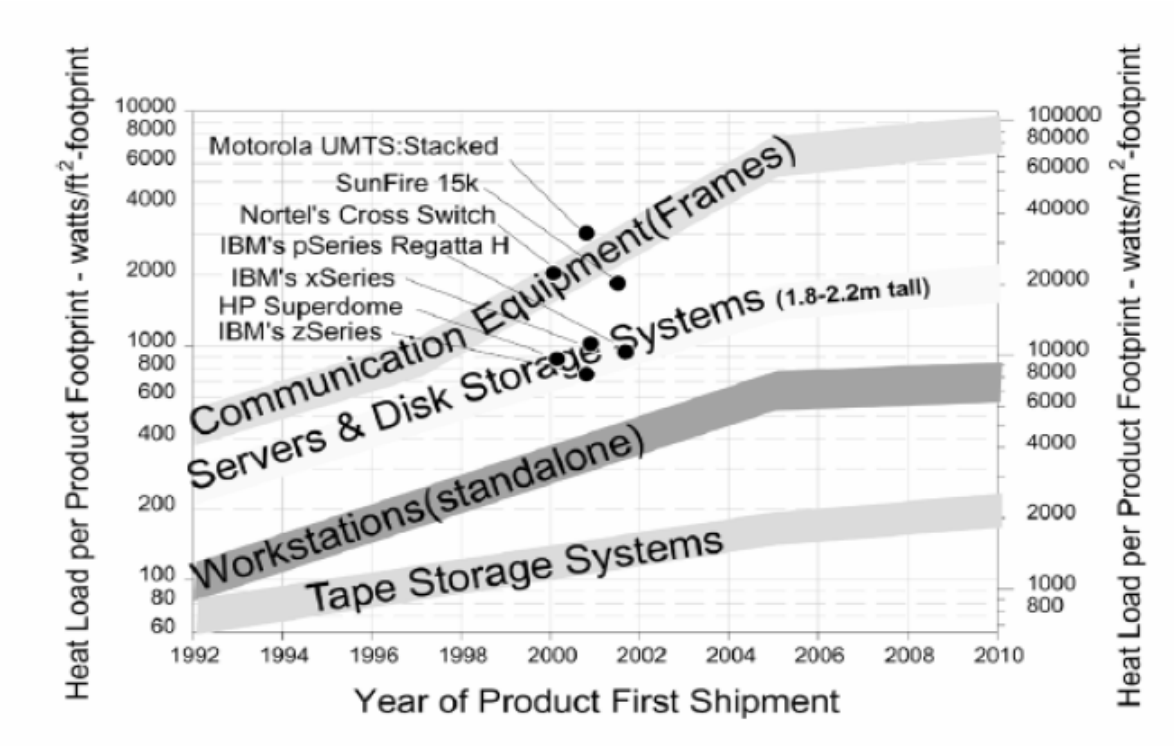

Fig. 1.6. Heat load per product foot print.

1.4 Heat Sink

Heat sink is an environment or objects that absorbs heat and dissipates heat from another using thermal contact (either direct or radiant).

Application:-

1. Cooling electronics devices like microprocessors
2. Refrigeration
3. Heat engines

In common use, it is metal object brought in to contact with an electronic component's hot surface. In most cases, a thin thermal interface material mediates between the two surfaces. Microprocessors and power handling semiconductors are examples of electronics that need a heat sink to reduce their temperature through increased thermal mass and heat dissipations (primarily by conduction and convection and to a lesser extent by radiation).

1.5 Microchannel Heat Sink

Heat removal has become an important factor in the advancement of microelectronics due to drastically integrated density of chips in digital devices and increased current-voltage handling capability of power electronic devices.

For thermal management, various types of cooling methods for microelectronics devices have been developed. Examples include extended surface (fins), the highly parallel air and liquid impingement systems, modular internal conduction enhancement and indirect and direct liquid cooling with water and dielectric coolants. The implementation of manifold microchannel heat sink, cooling micro heat pipes, pool boiling, multiphase flow, liquid metal heat sink and microchannel heat sink are also proposed for the cooling solution in microelectronics.

Microchannel heat sinks remove heat 50 times more efficiently than conventional methods. However, one-layered microchannel heat sinks induce high temperatures which can produce thermal stress on the chips and packages. To avoid such high temperatures, a large

pressure drop is necessary which moves the coolant through the cooling channels more rapidly, thus requiring a larger, noisier pumping system. Multi-layered microchannel heat sinks have been developed with a current flow arrangement for cooling that is a substantial improvement over conventional one-layered microchannel heat sink designs. The thermal performance and the temperature distribution for these types of microchannels were analyzed and a procedure for optimizing the geometrical design parameters was developed. While the power supply system of the multi-layered design is not significantly more complicated than the one-layered design, the stream-wise temperature rise on the base of surface was substantially reduced.

At the same time, the pressure drop required for the multi-layered heat sink was substantially smaller than the one-layer design. It is shown that the thermal resistance is as low as 0.03 ^{o}C/W for microchannel heat sinks, which is substantially lower than conventional channel-sized heat sinks. Microchannels having a dimension of sub-millimeter scale surely provides comparatively high heat transfer rate than in a conventional-sized channel, which is particularly beneficial to high end electronics cooling.

Generally, microchannel cooling method is compact with high heat transfer rate due to large surface area to volume ratio. Researchers showed that the heat transfer coefficient is inversely proportional to the channel hydraulic diameter.

Microchannels are advantageous due to its possibility in Multi-chip Module integration. Integrated circuit fabrication techniques used in constructing a microchannel heat sink make the Multi-chip Module integration possible. As a result, microchannels cooling method provides a fully integrated, efficient, rugged and compact design. Implementation of cooling technology using microchannels can remarkably reduce the contact thermal resistance in the cooling section, which is considered as the main cause of cooling rate increase.

1.5.1 Design Parameters

The design parameters include the heat sink material, the number and geometry of the fins and their alignment and the base plate thickness as shown in Fig. 1.7. In order to obtain the minimum thermal resistance and pressure drop, each of these parameters must be designed well.

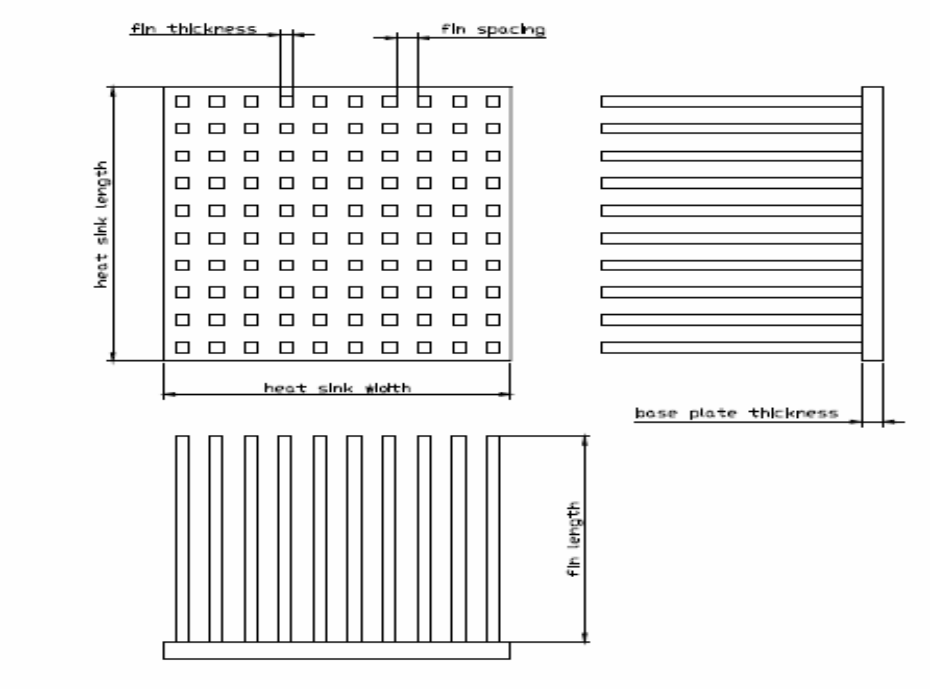

Fig. 1.7. Heat sink design parameters.

1.5.2 Heat Sink Material

Heat sinks are made from a good thermal conductor such as copper or aluminum alloy. Copper (401 W/m-K at 300 K) is significantly more expensive than aluminum (237 W/m-K at 300 K) but is roughly twice as efficient as thermal conductor. Aluminum has the significant advantage that it can be easily formed by extraction, thus making complex cross-sections possible. Aluminum is also much lighter than copper, offering less mechanical stress on delicate electronic components. Some heat sinks made from aluminum have a copper core as shown in Fig. 1.8. Although the thermal conductivity of zinc is lower compared to that of aluminum and copper, it may also be a good material for electronic cooling purposes. When zinc added to an alloy, it

eliminates porosity in the casting process, which is an advantage over aluminum and copper since they are not pore free after the casting.

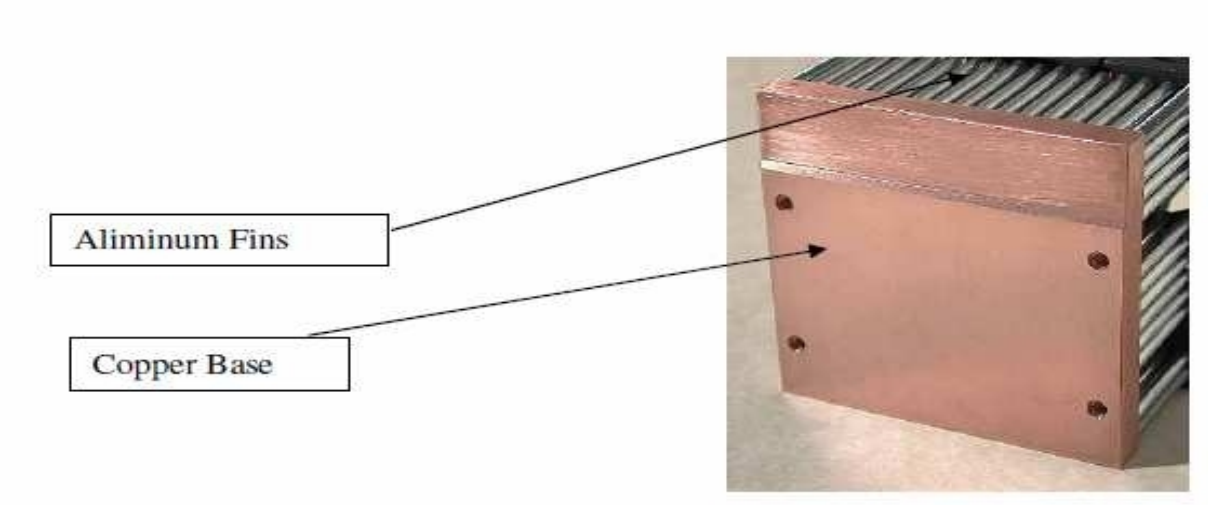

Fig. 1.8. Aluminum fins with copper base heat sink.

1.5.3 The Number of Fins

A heat sink usually consists of a base with one or more flat surfaces and an array of comb or fin-like protrusions to increase the heat sink's surface area contacting the air, and thus increasing the heat dissipation rate.

It is one of the most important factors for heat sink performance. A heat sink designed for electronics cooling is a compact heat exchanger for which the ratio of heat transfer area to occupied volume is very large. Therefore increasing the number of fins provides more area for heat transfer. Increasing the number of fins from 238 to 294, increased the heat transfer area by 8.4 %. However, it should be noted that increasing the number of fins creates an adverse effect, which is the increased static pressure drop. In order to overcome higher pressure drops, higher pumping powers are needed, which requires the installation of more powerful fans or blowers.

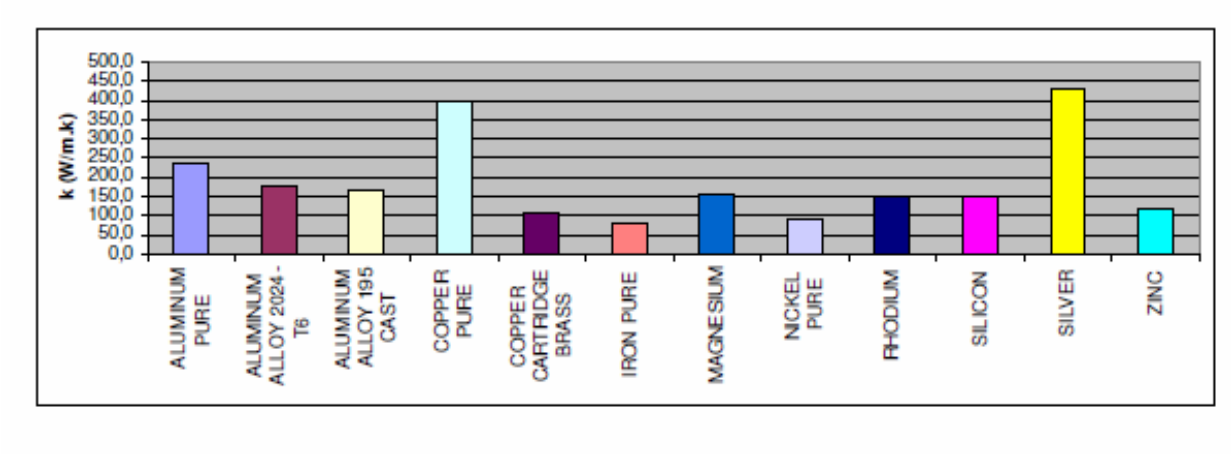

Fig. 1.9. Thermal conductivities of common heat sink materials.

1.5.4 Fin Shapes

Different kinds of heat sink geometries are possible. Pin fins (spines), uniform straight fins, tapered straight fins, splines and annular fins are possible. The most common ones are pin fins whose cross-section can be round, square, elliptical, hexagonal or any other suitable geometry. Straight fins that have rectangular cross sections are widely used. Depending on the spacing among the fins of a heat sink, flow requirements and pressure drops may differ. Design engineers try to achieve the minimum thermal resistance with the pressure drop as low as possible by modifying the fin shapes.

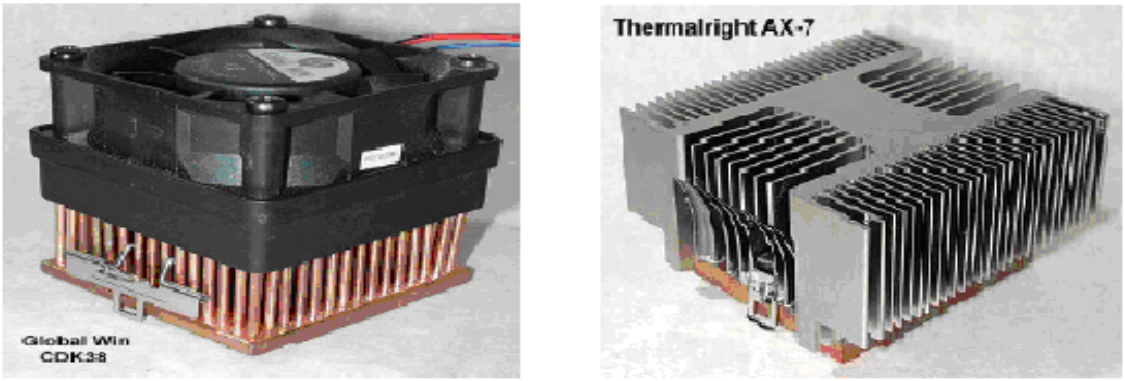

Fig. 1.10. Two heat sinks with different fin geometry.

1.5.5 Heat Transfer from Extended Surfaces (Fins)

Whenever the available surface is found inadequate to transfer the required quantity of heat with the available temperature drop and convective heat transfer coefficient, extended surfaces or fins are used. The following assumptions are made for the analysis of temperature distribution and heat flow through the fin:

(a) Steady state heat conduction.
(b) No heat generation within the fin.
(c) Uniform heat transfer coefficient over the entire surface of the fin.
(d) Homogeneous and isotropic fin material (i.e. thermal conductivity of material constant).
(e) Negligible contact thermal resistance.
(f) Heat conduction one-dimensional.
(g) Negligible radiation.

1.6 Background of Theory

1.6.1 Slip flow

A situation in which mean free path of a gas is between 1 and 65 % of the channel diameter, the gas layer next to the channel wall assumes a velocity of slip past the liquid, known as slip flow.

1.6.2 Knudsen number

It is a dimension less number, defined as the ratio of the molecular mean free path length to a representative physical length scale.

$$k_n = \frac{\lambda}{L}$$

1.6.3 Thermal accommodation coefficient

It is the fraction of heat transferred between the surface and molecule. If a particle of 900 K and it impacts the wall of 300 K the wall will heat up and the particle will cool down by

fraction of thermal accommodation coefficient. In the simulation the wall is assumed to be heat sink, meaning that the temperature never changes significantly.

1.7 Objective of the Work

The micro-heat sink modeled consists of a 10 mm long silicon substrate have a width of 57 µm and a depth of 180 µm has been analyzed. This numerical model with fully developed laminar flow used to analyze the heat transfer in a microchannel heat sink for different pressure drop. The numerical model is based on three dimensional conjugate heat transfer (2D fluid flow and 3D heat transfer). The main objective of the current work is

- to simulate the single microchannel heat sink for different pressure drop.
- to predict velocity, pressure and temperature profiles for constant heat flux on the chip.
- to predict temperature distribution along the channel.
- to define average heat transfer coefficient and Nusselt number for different pressure drop at constant heat flux and different heat flux.
- to define average heat flux distribution for different pressure drop at different walls of microchannel.

This will provide clear insight to the present work with the help of commercial CFD software i.e. FLUENT 6.2.16. The numerous grid generation technique implemented in GAMBIT is also successfully implemented for 2-D and 3-D domain. Both pre and post processing results of GAMBIT and FLUENT are utilized successfully during the simulation of the present situation. Furthermore, the results are also in good agreement with the available results.

1.8 Organization of the Thesis

Microchannel liquid cooling technique has emerged as an efficient thermal management technique for microelectronics as the requirement of cooling is moving beyond the limit of conventional air cooling technique.

This thesis has been organized in total five chapters. Chapter 1-2 is for foundation of the subject; chapter-3 is for mathematical formulation; while chapter-4 is for results and discussions and at last chapter-5 is for conclusions and scope for further work.

Chapter-1 contains the introduction to the subject of different types of chip cooling process at the chip level, module level and data center level. Wide varieties of methods that are used in industry are discussed here.

Chapter-2 contains literature survey, which presents a variety of research results done regarding chip cooling. This chapter is classified as numerical analysis, analytical results and experimental investigation.

Chapter-3 in this chapter mathematical formulation of the problem has been discussed. The computational domain and the boundary conditions are also discussed here.

Chapter-4 here the result outputs are discussed. Different contours and velocity profiles are presented in this chapter.

Chapter-5 contains the final conclusions and the scope of further
Appendix shows the detailed procedure of GAMBIT and FLUENT with the same geometry and boundary conditions.

CHAPTER 2

Literature Review

- ***Introduction***
- ***Analytical studies***
- ***Numerical studies***
- ***Experimental studies***
- ***Closure***

2.1 Introduction

Among the novel methods for thermal management of the high heat fluxes found in microelectronic devices, microchannels are the most effective at heat removal. The possibility of integrating microchannels directly in to the heat generating substrates makes them particularly attractive. The two important objectives in electronics cooling, minimization of the maximum substrate temperature and reduction of substrate temperature gradients can be achieved by the use of microchannels.

A large number of recent investigations have undertaken to study the fundamentals of microchannel flow as well as to compare the flow and heat transfer characteristics of microchannels with conventional channels. A comprehensive review of these investigations conducted over the past decade is presented in this chapter.

Studies on microchannel flows in the past decade are categorized in to various topics such as temperature, heat transfer in microchannels, Nusselt number, heat flux, comparison with flow in conventional channels, investigation of single phase and two-phase flows in microchannels, minichannels and small tubes, gas flow in microchannels, analytical studies on microchannel flows and design and testing of microchannel heat sinks for electronics cooling.

This chapter can be broadly classified under three categories. The first part of the survey deals with analytical studies. The second part of the survey deals with the numerical studies and the third part of the survey deals with the experimental studies.

2.2 Analytical Studies

Non-uniform Temperature Distribution in Electronic Devices Cooled by Flow in Parallel MicroChannels, was discussed by Hetsroni et al. [1]. Two-Phase Flow Patterns in Parallel Microchannels was studied by Hetsroni et al. [2]. They analyzed the effect of geometry on flow and heat transfer, finding that an increasingly uniform heat flux resulted in an increased irregularity of temperature distribution on the chip surface.

Bau [3] conducted an optimization study to minimize the temperature gradient and the maximum temperature for microchannel heat sink. It was demonstrated that further reduction in maximum temperature and temperature gradient could be achieved by varying the cross-sectional dimensions of the microchannel. The penalty of this method is the dramatically increased pressure drop due to the acceleration along the flow direction.

Culham et al. [4] presented an analytical approach for characterizing electronic packages, based on the steady-state solution of the Laplace equation for general rectangular geometries, where boundary conditions are uniformly specified over specific regions of the package. The basis of the solution is a general three dimensional Fourier series solution which satisfies the conduction equation within each layer of the package. The application of boundary conditions at the fluid-solid, package board and layer-layer interfaces provides a means for obtaining a unique analytical solution for complex IC packages. They compared the values with published experimental data for both a plastic quad flat package and a multichip module to demonstrate that an analytical approach can offer an accurate and efficient solution procedure for the thermal characterization of electronic packages.

Davies et al. [5] presented the method to correct the thermal resistance of electronics components is to adjust the junction-to-ambient thermal resistance to account for operational conditions. For forced convection applications, they proposed two factors; the first accounts for any upstream aerodynamic disturbance and the second addresses purely thermal interaction. Thus if an upstream powered component interacts with a downstream component, the two factors are combined. They found that both factors may be quantified in terms of readily measured temperatures and then used as coefficients to adjust the standard thermal resistance data for

operational conditions. They applied this approach to a symmetrical array of board mounted 160-lead devices and the data shows how the factors vary with component position, non-dimensional power distribution and Reynolds number. Based on data they proposed a new method of generating operational component thermal resistances.

Pucha et al. [6] presented a field-use induced damage mapping methodology that can take into consideration the field-use thermal environment profile to develop accelerated thermal cycling guidelines for packages intended to be used in military avionics thermal environment. They considered the board-level assembly process mechanics and critical geometric features with appropriate material models while developing the methodology. The models they developed are validated against in-house and published accelerated thermal cycling experimental data. The developed mapping methodology was employed to design alternate accelerated thermal cycles by matching the creep and plastic strain contributions to total inelastic strain accumulation in solder under military field-use and accelerated thermal cycling environments, while reducing the time for accelerated thermal cycling and qualification.

Zhao and Lu [7] presented an analytical and numerical study on the heat transfer characteristics of forced convection across a microchannel heat sink. Two analytical approaches are used by them: the porous medium model and the fin approach. In the porous medium approach, the modified Darcy equation for the fluid and the two-equation model for heat transfer between the solid and fluid phases are employed. Firstly, the effects of channel aspect ratio and effective thermal conductivity ratio on the overall Nusselt number of the heat sink are studied in detail. The predictions from the two approaches both show that the overall Nusselt number increases as aspect ratio increased and decreases with increasing thermal conductivity. The effect of porosity on the thermal performance of the microchannel was also examined by them. They found that, whereas the porous medium model predicts the existence of an optimal porosity for the microchannel heat sink, the fin approach predicts that the heat transfer capability of the heat sink increases monotonically with the porosity. They also studied the effect of turbulent heat transfer within the microchannel, and they found that turbulent heat transfer results in a decreased optimal porosity in comparison with that for the laminar flow. They proposed a new concept of microchannel cooling in combination with micro heat pipes, and the enhancement in heat transfer due to the heat pipes is estimated. Finally, they conducted two-dimensional numerical

calculations for both constant heat flux and constant wall temperature conditions to check the accuracy of analytical solutions and to examine the effect of different boundary conditions on the overall heat transfer.

Chen et al. [8] developed an effective method for predicting and optimizing the thermal performance of heat sinks with Parallel-Plain fin under a given design constraint of pressure drop. They developed the thermal and hydrodynamic performance analyzers for PPF heat sinks. A screening experimental design using the Taguchi method has been performed to determine key factors that are critical to the design and screen out unimportant design factors; and a Response Surface Methodology is then applied to establish analytical models for the thermal resistance and pressure drop in terms of the key design factors with a CCD experimental design. By employing the Sequential Quadratic Programming technique, a series of constrained optimal designs can be efficiently performed. After comparing between these predicted optimal designs and those evaluated by the theoretical calculations the agreement they got was satisfactory.

Modeling of transport in microchannels can be divided in to two categories. In the first, method used for macro-scale channels are directly implemented to evaluate the performance of microchannel heat sinks. In the second category, new effects are taken into account to explain the deviation of the measured results from classical theory. The former range from simple 1-D models (Phillips [9]; Knight et al. [10]) to three dimensional conjugate studies (Weisberg and Bau [11] and Yin and Bau [12] and Fedorov and Visakanta [13]). However, existing analytical studies are still inconclusive.

2.3 Numerical Studies

Mainfold microchannel heat sinks were first suggested in Harpole and Eninger [14] and numerically studied by Copeland et al. [15] and Ng et al. [16]. Compared to conventional microchannel heat sinks, manifold microchannel heat sinks feature many inlet and outlet manifolds, alternating at a periodic distance along the length of the microchannels. Coolant flows from the inlet port in to the manifolds and forms separate streams. Each stream flows through a short section of microchannels. If fully developed laminar flow fixed flow rate are assumed, at the pressure drop is reduced by a factor equal to the number of manifold inlet/outlet compared with conventional microchannel heat-sink, on the other hand the same temperature variation exists for manifold microchannel in a much shorter distance. There are also concerns on the heat transfer efficiency for the region underneath the manifolds.

Hung et al.[17] performed numerical simulations to investigate convective-conductive heat transfer due to a laminar boundary layer flow of air over a two dimensional array of rectangular chip blocks which represent the finite heat sources. A time-accurate numerical scheme algorithm, PISO (pressure-implicit with splitting of operators), has been used to simulate the conjugate heat transfer between the fluid and solid phases. The results of the simulations show that the existence of the array of blocks results in stagnant flow regions between blocks in which heat converted to the ambient flow field is limited. It was found that heat transfer can be enhanced passively, especially in the areas between blocks, by opening the chip board between blocks. The enhancement of heat transfer thus occurring is presumably due to a pseudo-suction force which induces a vertical flow between blocks. The enhancement of heat transfer for the chips on-board is reflected by a global increase of the Nusselt number on the chip blocks, especially on the west sides of the chips located further downstream of the flow direction. Further investigation shows that the chip-to-chip temperature variations diminish if the openings located upstream of the front end block and downstream of the rear end block are sealed. The optimal cooling configuration for the array of chip blocks can be utilized by the electronics industry.

Li et al. [18] numerically simulated a forced convection heat transfer occurring in silicon based micro channel heat sinks has been conducted using a simplified three-dimensional conjugate heat transfer model (2D fluid flow and 3D heat transfer) consists of a 10 mm long silicon substrate,

with rectangular micro channel, 57 µm wide and 180 µm deep, fabricated along entire length with hydraulic diameter 86 µm. The influence of the geometric parameters of the channel and thermo physical properties of the fluid on the flow and the heat transfer, are investigated using temperature dependent thermo physical property method. Result indicates that these properties of the liquid can significantly influence both the flow heat transfer in the micro channel heat sink. The result indicates that the variations in the way the Nusselt number is defined may results in different conclusions even using the same experimental data. The numerical results are then compared with other published numerical results and experimental data available in literature.

Masud et al. [19] tried to validate the CFD package FLUENT with the experimental data obtained by then earlier. Here they have taken a heated chip with temperature 353 K and the air inlet velocity at temperature 293 K. The inlet velocities were varied from 1 m/s to 7 m/s. Various turbulence models have been tested, and the effect of the channel inlet flow on the heat transfer rate has been determined by considering both a uniform and fully-developed condition. The substrate adiabatic heat transfer rate has been determined by considering both uniform and fully-developed condition. The substrate adiabatic heat transfer coefficient is also numerically determined. The results indicate that the flow in the vicinity of the module is three dimensional, and exhibits flow separation and vortex formation, hence leading to a complex distribution of the local heat transfer coefficient on the substrate. In general the flow structure was in good agreement with the experiments. The predicted turbulence intensity did not agree well with the measurements. The turbulence treatment near the wall is very important and wall functions are not suitable.

Dhiman et al. [20] investigated the flow and heat transfer characteristics of an isolated square cylinder in cross-flow placed symmetrically in a planar slit for a range of conditions. They obtained the heat transfer correlations in the steady flow regime for the constant temperature and constant heat flux boundary conditions on the solid square cylinder in cross-flow. In addition, variation of the local Nusselt number on each face of the obstacle and representative isotherm plots are presented to elucidate the role of Prandtl number and blockage ratio on drag coefficient and heat transfer.

Cheng et al. [21] numerically investigated the fluid flow and heat transfer characteristics of mixed convection in three-dimensional rectangular channel with four heat sources. The SIMPLEC algorithm was applied to deal with the coupling between pressure and velocity, and new high-order stability guaranteed second-order difference scheme was adopted to discretize the convection term. They studied the influence of four parameters: Richardson number, heat source distribution, channel height and inclination angle. They analyzed the numerical results from the viewpoint of the field synergy principle, which says that the enhanced convective heat transfer is related not only to the velocity field and temperature field, but also to the synergy between them. They found that the effects of the four parameters on the thermal performance can all be explained with the field synergy principle. To obtain better electronic cooling, the synergy between the velocity and temperature gradient should be increased when other conditions are unchanged.

Kumara et al. [22] investigated the complex unsteady flow through and around a channel in the presence of an obstruction at the entry is studied by solving directly the unsteady Navier-Stokes equations. They considered the Reynolds number of 4000, as experimental results is available for comparison. The computed results are in close agreement with experiments. The computations help with better understanding of the phenomenon of reverse flow and fluid pumping.

Roy and Bandyopadhyay [23] conducted a similar type investigation by developing a fully explicit two-dimensional incompressible laminar Navier-Stokes solver in primitive variable formulation using a Cartesian staggered grid. The governing equations have been solved on the physical plane using a finite volume discretization scheme. They discretized the convective terms of the solver using the weighted second upwind SOLA scheme. The pressure is solved by using the SOLA pressure correction algorithm. The diffusive terms of the momentum equations are discretized by using central differencing scheme. In their investigation, flow past a square cylinder placed inside a channel with two different blockage ratios, namely, 0.125 and 0.250 have been computed at four different Reynolds numbers, namely, 150, 300, 750 and 1500. The average drag coefficient increases with an increase in blockage ratio for a given Reynolds number. The vortex shedding frequency also increases with increase in blockage ratio. Recirculation zones are formed on the channel wall surfaces for Reynolds numbers 750 and 1500, respectively. Recirculating zones on the walls are affected by the vortex shedding process.

Their structure and location get modified from time to time. Streamlines, velocity contours and pressure contours are provided to analyze the important characteristics of the flow field.

Rodgers et al. [24] assessed the numerical predictive accuracy for PCB heat transfer in forced convection using a widely used CFD software, as component junction temperature prediction accuracy for the populated board case is typically within 65 °C or 610 %, which would not be sufficient for temperature predictions to be used as boundary conditions for subsequent reliability and electrical performance analyses. Neither the laminar nor turbulent flow model resolves the complete flow field, suggesting the need for a turbulence model capable of modeling transition. They show that the full complexity of component thermal interaction is not to be fully captured.

Heat transfer phenomenon in microchannel heat sinks using three-dimensional numerical analysis was investigated by Qu and Mudawar [25] and Ryu et al. [26] this paper presents the three-dimensional fluid flow and heat transfer in a rectangular microchannel heat sink are analyzed numerically using water as the cooling fluid. A numerical code based on the finite difference method and the SIMPLE algorithm is developed to solve the governing equations. By investigation it is found that the temperature rise along the flow direction in the solid and fluid regions can be approximated as linear. The highest temperature is encountered at the heated base surface of the heat sink immediately above the channel outlet. The heat flux and Nusselt number have much higher values near the channel inlet and vary around the channel periphery, approaching zero in the corners. For a relatively high Reynolds number of 1400, fully developed flow may not be achieved inside the heat sink. Increasing the thermal conductivity of the solid substrate reduces the temperature at the heated base surface of the heat sink, especially near the channel outlet.

In an attempt to counter current flow arrangement for the cooling of electronic components Vafai and Zhu [27] compared the thermal performance of two layer microchannel heat sinks with single layer conventional heat sinks. It was found that counter-flow arrangement reduces the temperature gradient dramatically compared with single-layered microchannel for Re = 143.6. This work shows a new concept for a two-layered microchannel heat sink with counter current flow arrangement for cooling of the electronic components is proposed. The thermal performance and temperature distribution for these types microchannels were analyzed and a

procedure of optimizing the geometrical design parameters is presented the streamwise temperature rise on the base surface was found to be substantially reduced compared to that of the one-layered heat sink. At the same time the pressure drop required for the two-layered heat sink was found to be substantially smaller than that of the one-layered heat sink. The results demonstrate that the two-layered microchannel heat sink design is a substantial improvement over the conventional one-layerd microchannel heat sink. This study is focused on the temperature distribution, thermal resistance and the optimization of geometrical design parameters.

FLUENT, a computational fluid dynamics (CFD) program was used to predict the temperature distribution in a microchannel heat exchanger. The results from the numerical simulation were then compared to experimental data. The experimental data was gathered by monitoring a single 0.31 mm x 10 mm cross-section microchannel chip that was cooled using water flow convection. The chip was heated by applying voltage to an aluminum heater, and temperatures from 40 ^{o}C to 120 ^{o}C were observed using an infrared camera, it has been determined that higher flow rate is better for convection. The results also demonstrated that an increase in the use of a high mass flux improves single-phase convection flow. The experiment illustrated that the thermal resistance is independent of the heat flux values.

Pfund et al. [28] performed numerical simulations to investigate convective-conductive heat transfer due to a laminar boundary layer flow of air over a two dimensional array of rectangular chip blocks which represent the finite heat sources. A time-accurate numerical scheme algorithm, PISO (pressure-implicit with splitting of operators), has been used to simulate the conjugate heat transfer between the fluid and solid phases. The results of the simulations show that the existence of the array of blocks results in stagnant flow regions between blocks in which heat converted to the ambient flow field is limited. It was found that heat transfer can be enhanced passively, especially in the areas between blocks, by opening the chip board between blocks. The enhancement of heat transfer thus occurring is presumably due to a pseudo-suction force which induces a vertical flow between blocks. The enhancement of heat transfer for the chips on-board is reflected by a global increase of the Nusselt number on the chip blocks, especially on the west sides of the chips located further downstream of the flow direction. Further investigation shows that the chip-to-chip temperature variations diminish if the openings located upstream of the

front end block and downstream of the rear end block are sealed. The optimal cooling configuration for the array of chip blocks can be utilized by the electronics industry.

2.4 Experimental Studies

Microchannel heat sink was first proposed for heat sinking of VLSI electronic components in 1980s. Tukerman and pease [29] Tuckerman and Pease [29] used silicon microchannels, with water as the working fluid, to dissipate power from an electronic chip. The microchannels were etched in a silicon sample with an overall dimension of $1cm^2$. They had a channel width of approximately 60 μm and a parameterized channel height varying between 287 μm and 376 μm. These microchannels effectively dissipated heat up to 790 W/cm^2 while maintaining a chip temperature below 110 °C.

Wong and Peck [30] evaluated experimentally the effect of altitude on electronic cooling. As material properties of air vary as a function of altitude due to changes in atmospheric pressure and temperature, these changes have a negative impact on the heat transfer effectiveness and result in higher component temperature when compared to sea level conditions. They carried out the experiments in a hypobaric chamber using electronic printed circuit boards populated with heated rectangular blocks placed in a small wind tunnel. The altitude was varied between 0 and 5000 m above sea level and the air speed is varied between 1 and 5 m/s. The results show the local adiabatic heat transfer coefficient and thermal wake function diminish with altitude. This information is useful for design and analysis of electronic equipment for operation over a range of altitudes and air speeds typically encountered in forced air convection cooling applications.

Haider et al. [31] studied a model for the two-phase flow and heat transfer in the closed loop, two-phase thermosyphon involving co-current natural circulation. The focus was on CLTPTs for electronics cooling that exhibit complex two-phase flow patterns due to the closed loop geometry and small tube size. They used homogeneous two-phase flow model to evaluate the friction pressure drop of the two-phase flow imposed by the available gravitational head through the loop. They used the boiling characteristics of the enhanced structure to predict the chip

temperature. The comparison with experimental data for dielectric working fluid PF-5060 and was in general agreement with the observed trends.

Yoo et al. [32] investigated how the flow via an obstruction in forced convection influence the local heat transfer from electronic modules. They have conducted experiments on a three-dimensional array of hexahedral elements as well as on a two-dimensional array of rectangular elements. Naphthalene sublimation technique was employed to measure three-dimensional local heat and mass transfer data are converted to their counterparts of the heat transfer process using the analogy equation between heat and mass transfer. Module location and stream wise module spacing were varied, and the effect of vortex generators on heat transfer enhancement was also examined. The results show dramatic change of local heat transfer coefficients on each surface of the module, and three-dimensional modules have a little higher heat transfer value than two-dimensional modules because of bypass flow. Longitudinal vortices formed by vortex generator enhance the mixing of fluids and thereby heat transfer, and the rectangular wing type vortex generator is found to be more effective than the delta wing type vortex generator.

Rhee et al. [33] estimated experimentally the continuous, one-dimensional kernel function in a rectangular duct subject to forced convection with air using liquid crystal tomography techniques. They manipulated the analytical relationships between the kernel function for internal flow and the temperature distribution resulting from a known heat flux distribution to accomplish this objective. They proposed a model for the kernel function in the hydrodynamic entry region of the rectangular duct, and used in its experimental determination. The kernel functions obtained by the work were shown to be capable of predicting the highly non uniform surface temperature rise above the inlet temperature resulting from an arbitrary heat flux distribution to within the experimental uncertainty. This is better than the prediction obtained using the analytically derived kernel function for turbulent flow between parallel plates, and the prediction obtained using the conventional heat transfer coefficient for constant heat flux boundary conditions. The latter prediction fails to capture both the quantitative and qualitative nature of the problem. The results of their work are relevant to applications involving the thermal management of non uniform temperature surfaces subject to internal convection with air, such as board level electronics cooling.

DeVoe and Ortega [34] performed a systematic study of the influence of board conduction on the predictive accuracy of Compact Thermal Models of BGA and CPGA package styles. Various resistance network topologies were assessed by them for each package style. They created the detailed (FE) isotropic board models with conductivities spanning three orders of magnitude to test the influence of board conductivity on CTM accuracy. They compared the results to equivalent fully-detailed (FE) package models on detailed board models. The predictive capability of the optimized topologies was strongly correlated to the existence of strong local temperature gradients in the board, whenever the sensitivity to board heat conduction was high. When the board is poorly conducting (k = l W/m-K), board heat conduction is too low to matter. When the board is highly conducting (k = l00W/m-K), the high conductivity smoothes out local board temperature gradients, and the CTMs are accurate even though the board heat flow path is dominant. In general, they found that optimized network topologies that included shunt resistances to predict the junction temperature to within 5 % to 8 % over a wide range of board conductivities, while star-shaped networks were generally only accurate to 10-15 %.

Following the work of Tuckerman and Pease [29] many studies have been performed to characterize flow and heat transfer in microchannel structures. Friction factor Nusselt number are the two primary parameters examined in most of the experimental literature. Wu and Little [39] tests for flow of gas in trapezoidal microchannels and the found the friction factor for laminar flow in microchannel to be generally larger than predicted by the Moody diagram and to be affected by surface roughness. They also found that the Nusselt number varied with Reynolds number in the laminar regime. This was one of the first studies that predicted a higher Nusselt number for microchannels when compared to macroscale equations Pfahler et al. [35] however found the friction factor for microchannels to be smaller than predicted by laminar theory.

The single phase forced convective heat transfer and flow characteristics of water in micro channel structures/plates with small rectangular channel hydraulic diameters of 0.133-0.367 mm and distinct geometric configurations were investigated experimentally by Peng and Peterson [36]. The laminar heat transfer was found to be dependent upon the aspect ratio and the ratio of hydraulic diameter to the center-center distance microchannel. The flow resistance of the liquid flow in the microstructures was also investigated experimentally and analytically, and correlations were proposed for the calculation of the flow resistance.

Experimental investigation on liquid forced convection heat transfer through microchannels was studied by Peng and Wang [37] the experiments were conducted to investigate the single phase forced flow convection of water methanol flowing through microchannels with rectangular cross-section. The transition and laminar heat transfer behavior on microchannels are very unusual and complex and are strongly affected by liquid temperature, velocity and microchannel size. The reported deviations were attributed to different sources such as micro-rotational effects of the molecules (Papautsky et al [38]), surface roughness (Mala and Li [39]), electric double layer (Mala et al [40]) and viscous heating (Tso and Mahulikar [41]).

Xu et al. [42] reported that flow characteristics in microchannels with hydraulic diameter of 30 to 34µm at Reynolds numbers of 20 to 4000 agree with predictions based on the Navier-stocks equation. Liu and Garimella [43] showed that conventional correlations offer reliable predictions for laminar flow characteristics in microchannels over a hydraulic diameter range of 240 to 974µm.

Recently Lee and Garimella [44] investigated heat transfer in microchannels made of copper for Reynolds number 300 to 3500. The width of the studied channels range from 194 to 534 µm while the depths are five times the widths. In deducing the average Nusselt number, an average wall temperature based on a one-dimensional conduction model was used. For laminar flow the measured Nusselt number agreed with predictions for thermally developing flow over the entire length of the channel. They found that a classical macroscale analysis can be applied to microchannels, although care must be taken to use the proper theoretical or empirical correlation. Many of the empirical correlations available did not match with their experimental data. However, their numerical analysis showed good agreement with their experimental results in the laminar regime. They indicated that considerations of entrance regions and turbulent transitions must be accounted for.

Baviere et al [45] studied flow inside smooth and rough microchannels with height range of 7µm to 300µm and Reynolds number range of 0.01 to 8000. In the smooth wall case, the result of friction factor was well predicted by theory. For the rough wall case, an artificial surface roughness was added to the side wall of the smooth microchannels and measured friction loss was significantly larger but no earlier transition to turbulence was observed.

Developing convective heat transfer in deep rectangular microchannel was experimentally investigated by Harms et al. [46]. Here two configuration were tested, a single channel system and a multiple channel system. The results show that, in terms of flow and heat transfer characteristics, our microchannel system designed for developing laminar flow outperforms the comparable single channel system designed for turbulent flow.

Choi et al. [47] also suggested from their experiments with microchannels that the Nusselt number did in fact depend on the Reynolds number in laminar microchannel flow. They also found that the turbulent regime Nusselt numbers were higher than expected from the Dittus-Boelter equation. Rahman and Gui [48, 49] found Nusselt numbers to be high in the laminar regime and low in the turbulent regime as compared to theory Jung and Kwak [50], Lee and Garimella [51]. Similar to Choi et al [47] found that their measured Nusselt numbers in the turbulent regime were higher than the Dittus-Boelter equation. Adams et al. [52] tested microchannels in the turbulent regime and found their results to be higher than predicted by theoretical turbulent equations. Nusselt numbers in excess of theoretical predictions were also found by Celata et al. [53] and Bucca et al. [54] through experimental work with microchannels.
Harms et al. [55] performed experiments on an array of microchannels and determined that local Nusselt numbers can be accurately predicted in microchannels by conventional correlations. They also determined that proper plenum design and consideration are necessary to be able to apply the theoretical Nusselt number and friction factor equations to microchannel experiments.
Qu and Mudawar [56] performed both experimental and numerical studies on microchannels with 231 μm widths and 713 μm depths. They tested only in the laminar regime, and they indicated that the Navier Stokes and energy equations do in fact properly predict fluid flow and heat transfer in microchannels. Owhaib and Palm [57] tested channels with diameters ranging from 800 μm to 1700 μm, and found good agreement with theory for Nusselt number in the turbulent regime.

Kohl et al. [58] measured pressure drop in microchannels through internal pressure measurements. They constructed microchannel tap lines of 7 μm width and 10 μm depth using microfabrication techniques. Their results showed that both friction factor and turbulent transition Reynolds numbers agreed well with theoretical results. It should be noted, however,

that their tests which used water as a working fluid were conducted in relatively smooth channels.

Zeighami et al. [59] measured transition using the repeatability of velocity data and particle motion. Their results showed a transition region in the range of Reynolds numbers from 1200-1600 [60] and Lee et al [61] defined the onset of turbulence through deviations in velocity profiles, and they found the critical Reynolds number to be 2900 [60].

Guo and Li [60] indicated from their experiments on microchannels with high relative roughnesses that friction factors increased with relative roughness, and they also proposed that wall roughness effects may incur early turbulence transition and higher than expected Nusselt numbers. Tu and Hrnjak [62] performed friction factor experiments on smooth microchannels, and they found that their results were well predicted by laminar theory.

Sharp and Adrian [63] performed MicroPIV experiments on glass tubes, and they identified transition through the presence of unsteady changes in centerline velocity. Their findings more closely relate to conventional theory, with critical Reynolds numbers ranging from 1800 to 2200.

Lior et al. [64] performed similar studies on microchannels with transition criteria defined also with deviations in centerline velocity, and they found the transition Reynolds number to be 1535. They also found that the fully turbulent region began at Reynolds numbers of 2630 to 2853.

Li and Olsen [65, 66] performed MicroPIV visualizations on microchannels and determined that no early transition to turbulence was present in their studies. Some of their investigations included microchannels with hydraulic diameters of 320 μm and aspect ratios of 1 to 5.7 being tested over a Reynolds number range of 200 to 3267. They quantified the onset of turbulence by an increase in centerline velocity fluctuations, and they found that the transition region occurred for Reynolds numbers from 1765 to 2315. They also found that fully developed turbulent flow began to occur at Reynolds numbers ranging from 2600 to 3200. While many of the studies mentioned above involve only smooth microchannels, there has also been a good deal of research on the effects of roughness on friction factor and transition to turbulence.

Steinke and Kandlikar [67] they tested had a significant surface roughness, and a friction factor increase and transition Reynolds number decrease to 1570 was found for this case. As a summary of the information gathered on friction factor experiments conducted on microchannels, it can be said that conventional theory for macroscale conditions can be readily applied to smooth-wall microchannels. However, there is a great deal of investigation left to be done to make conclusions about the effects of surface roughness on both the friction factor and turbulent transition Reynolds number in microchannels.

Judy et al. [68] did pressure drop experiments on both round and square microchannels with hydraulic diameters ranging from 15 to 150μm. They tested distilled water, methanol and isopropanol over a Reynolds number range of 8 to 2300.

Kawano et al. [69] this investigation indicated that the average channel wall temperature along the flow direction was nearly uniform except in the region close to the channel inlet, where very large temperature gradients were observed. They are using a numerical method similar to that proposed by both. This model considered the hydrodynamic and thermal developing flow along the channel and found that the highest temperature is typically encountered at the heated based surface of the heat sink immediately adjacent to the channel outlet, and that the temperature rise along the flow direction in the solid and fluid regions can both be approximated as linear.

Pak et al. [70] and Kim et al. [71] that provide the experimental data for friction and heat transfer in the microchannels under conditions which are directly relevant to those found in the integrated circuits of modern electronic devices i.e., when the substrate (heat spreader) is highly conducting and massive in comparisons and therefore, the conjugate conduction-convection effects are important.

Tae hoji [72] performed experiments to investigate heat dissipation from a heated square cylinder in a channel by oscillating flow. During the experiments, the input power and oscillating amplitude (A) were fixed. The effects of the Reynolds number based on the mean flow velocity and the oscillating frequency on the heat transfer enhancement are examined. They determined the time averaged Nusselt number and the Strouhal number for each oscillating condition. The measured Strouhal numbers according to the Reynolds number are compared with the previous

results and good agreement is found. The occurrence of the “lock-on” phenomenon is demonstrated for a square cylinder. When the pulsating frequency is in the lock-on regime, the heat transfer from a square cylinder is dramatically enhanced. They found that the heat transfer enhancement is pronounced as the Reynolds number increases.

Wu and Little [73] it is pointed out that the shape of the entrance is very important, with much shorter entrance lengths occurring for square-edged entrances than for rounded ones. Thus because the flow entrance length may be less than 5% of the total length for a rectangular channel heat sink, the assumption of fully developed laminar flow over the entire length of the microchannel is acceptable for the heat transfer analysis, particularly in case such as this where the Reynolds number is less than 150. This assumption is verified by the experimental results of Kawano et al. [69].

2.5 Closure

Many research papers were published regarding electronics chip cooling. Some of them investigated analytically, some are numerically and rest experimentally predicted. The implementation of this technology is still in its infancy. Major obstacles in implementing this technology are due to the lack of substantial understanding in the behavior of microchannel system. There are many challenges in microchannel fluid mechanics and heat transfer study. Therefore, scientific approach in analyzing the fluid flow and heat transfer behavior in microchannel is essential in developing a viable cooling solution. Mostly analytical solutions are newly developed techniques which needs validations. Numerical solutions are, solving the governing equations by different techniques, or using the commercially available codes. But validating the codes is also an ongoing process, which is still going on. Finally the experimental investigation results are practically needed results. So the experimental results are also required to validate the CFD codes. In this study the governing equations has been solved by SIMPLE method and analyze the results obtained.

CHAPTER 3

Mathematical Formulation

- ***Introduction***
- ***Description of the Cooling Model***
- ***Computational Domain Generated by GAMBIT***
- ***Application of FLUENT 6.2.16 for Simulation of Microchannel Heat Sink***
- ***Governing Equations***
- ***Boundary Conditions***
- ***Closure***

3.1 Introduction

The three-dimensional fluid flow and heat transfer in a rectangular microchannels heat sink are analyzed using water as the cooling fluid. A schematic of the structure of a rectangular microchannel heat sink as shown in Fig. 3.1.The micro-heat sink model consists of a 10 mm long (L=10 mm) silicon wafer having a width of w = 57 µm, a depth of h = 180 µm and are separated by 43 µm wall thickness. A uniform heat flux is applied at the bottom surface of the heat sink. Heat transferred in the unit cell is a conjugate problem which combines heat conduction through the solid and dissipated away by convection of the cooling fluid in microchannel.

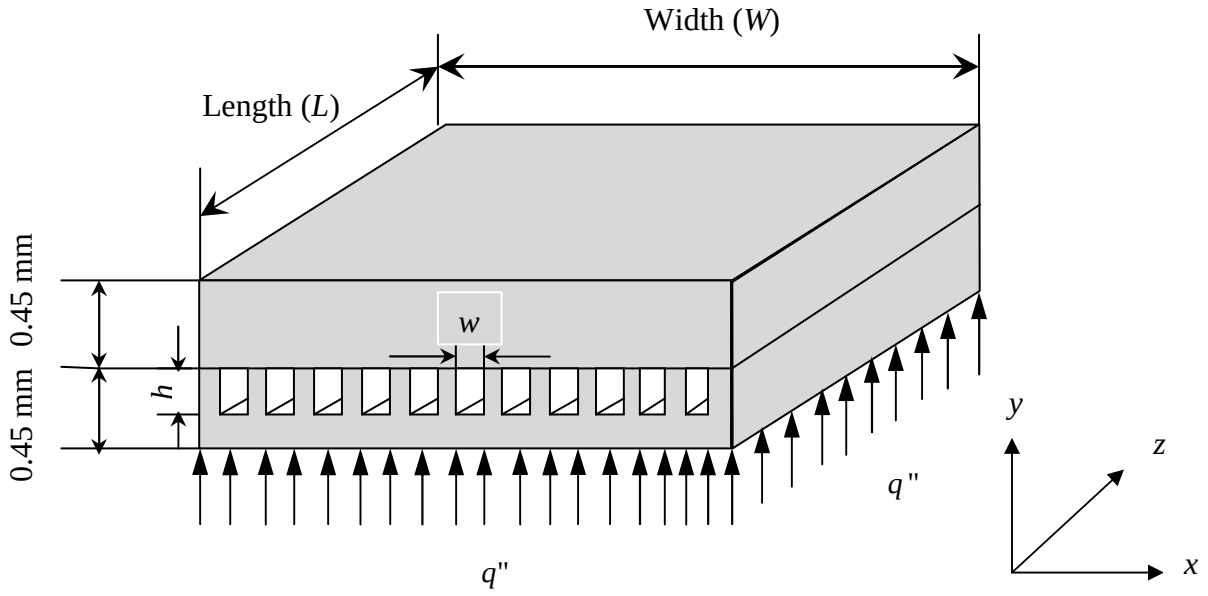

Fig. 3.1. Schematic of the microchannel heat sink.

3.2 Description of the Cooling Model

A rectangular microchannel of dimension (10 mm × 100 µm × 900 µm). Each channel has a height *h*, length *L* and width *w*. The bottom surface of heat sink at $y = 0$ is uniformly heated with a constant heat flux and at the top surface at $y = H$ is well insulated, also the adiabatic conditions are applied at the other boundaries. Fluid flowing through the channel at temperature 20 ^{o}C on account of pressure loss of 50 kPa. The direction of the fluid flow parallel to the *z*-axis as shown in Fig. 3.2. The flow is assumed to be laminar and both hydrodynamically and thermally fully developed. Also the thermophysical properties are assumed to be constant. The geometric dimensions of the microchannels with hydraulic diameter which was calculated from equation 3.12 of the microchannels are listed in Table 1.

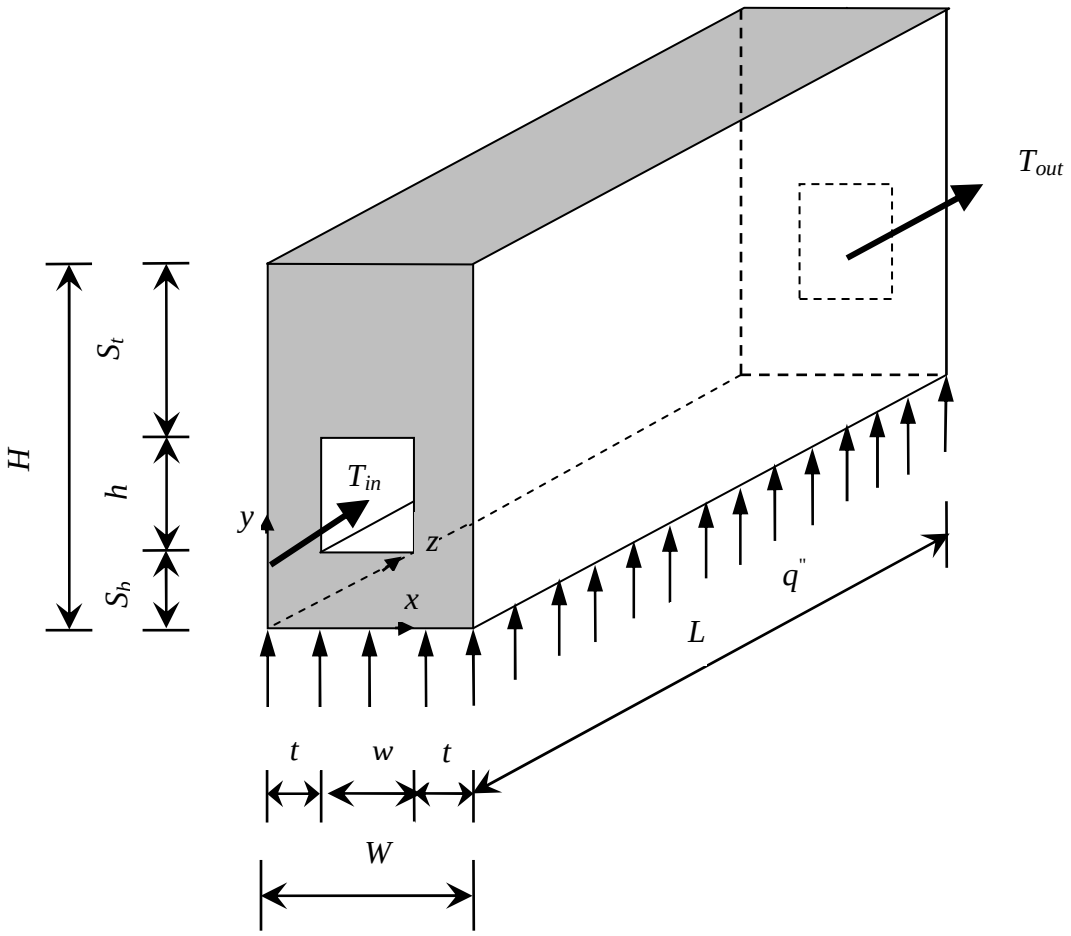

Fig. 3.2. Computational domain of microchannel heat sink.

H (μm)	h (μm)	W (μm)	w (μm)	S_t (μm)	S_b (μm)	t (μm)	L (mm)	D_h (μm)
900	180	100	57	450	270	21.5	10	86.58

Table 3.1 Geometric dimensions of the single microchannel.

3.3 Computational Domain Generated by GAMBIT

A numerical model was formulated to solve the three-dimensional heat transfer in microchannels using the commercial CFD software packages, FLUENT (FLUENT Inc., 1998). The microchannel is simulated to compare the results with available numerically simulated results by Li et al [18]. GAMBIT is a physical domain creation and discretization (meshing) soft ware, which is easily detected by 3-D FLUENT solver interface. The interior microchannel is meshed with double spacing technique as shown in Fig. 3.3 below. Then the 2-D face is generated by PAVE meshing technique. The 3-D meshing is done by using Cooper method of grid generation. The grid system has 10 nodes in the *x*-direction, 20 nodes in the *y*-direction and 50 nodes in the *z*-direction as in Fig. 3.3. The microchannel inner faces are declared as the walls and other walls are declared as walls with insulation boundary but the bottom most is declared as constant heat flux boundary. Similarly the microchannel is declared as the fluid zone and the rest is declared as solid zone. This declaration helps to detect and recognize in FLUENT for boundary condition and zone assignment. The mesh generated in the GAMBIT is exported to FLUENT 3-D solver after assigning the inlet, outlet and all the faces of the computational domain. The detail procedure of this model using GAMBIT and FLUENT was given in APPENDIX. The 2-D and 3-D grids are shown in following Fig. 3.3 and Fig. 3.4.

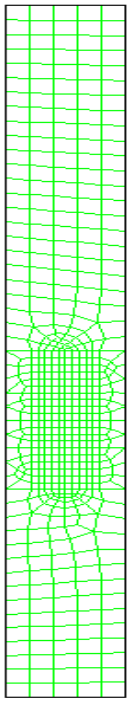

Fig. 3.3. PAVE meshing of the rectangular hollow solid channel surrounding the fluid region.

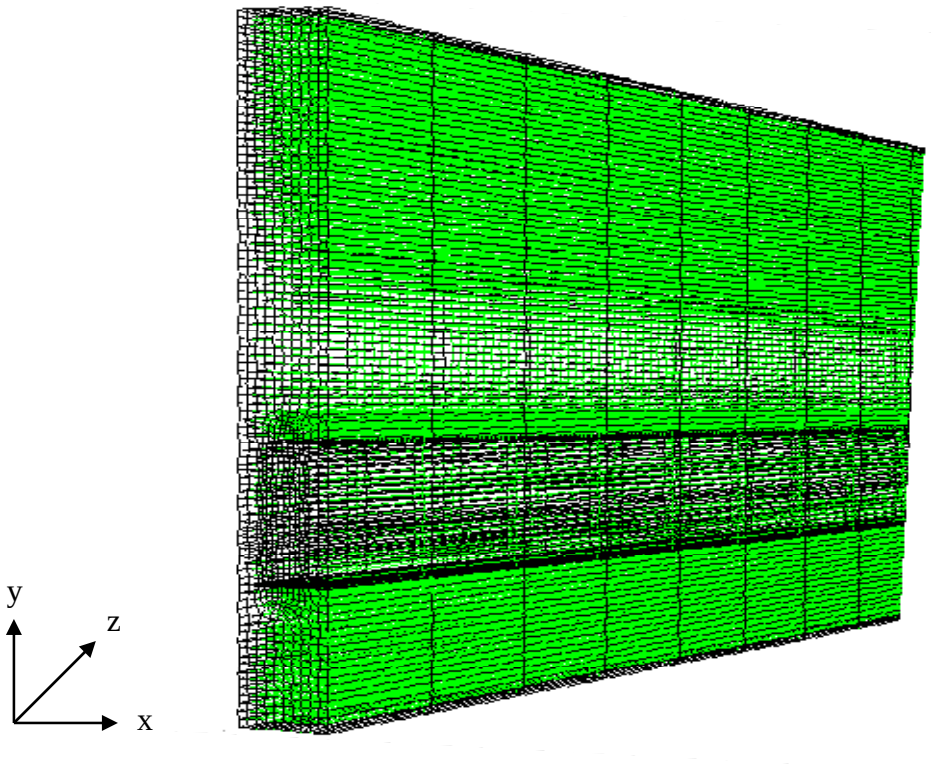

Fig. 3.4. Optimum grid system of complete model.

3.4 Application of FLUENT 6.2.16 for Simulation of Microchannel Heat Sink

The meshed and boundary assigned domain is exported to the fluent as mesh file. The 3-d solver is selected. The grid is checked and smoothed after proper scaling of the domain. The material and boundary conditions are selected from fluent database. The solver for laminar flow is selected for simulation purpose. The energy equation, operating conditions are also imposed. The simulation starts from the heat flux boundary with gravity along *y*-direction.

The second order upwind scheme is used to solve the combined convection-diffusion effect in the governing equations. The SIMPLE (Semi-Implicit Method for Pressure Linked equation) algorithm was then applied to solve the coupled systems of equations. In order to expedite the convergence of the calculations, the residuals for the continuity equation are smaller than 10^{-4} and the residual of the energy equation becomes less than 10^{-6} has been taken.

The Governing equations and the corresponding boundary conditions can be expressed as

3.5 Governing Equations

The governing equations are continuity, momentum and energy equations, which are derived from fundamental principles of heat and fluid flow. The equations are posed to implement SIMPLE (Semi-Implicit Method for Pressure Linked equation) algorithm. Here no-slip assumptions are made.

According to LANGHAAR EQUATION-

The length required to fully developed laminar flow entrance length = $0.057Re \times D_h$

$= (0.057 \times 105 \times 86.58)\ \mu m = 518.18\ \mu m < 10\ mm$

So fully developed laminar flow is valid.

Some simplifying assumptions are required before applying the conventional Navier-Stokes and energy equations to the model. The major assumptions are:

(1) steady state flow and heat transfer,
(2) incompressible fluid,
(3) laminar flow,
(4) uniform wall heat flux,
(5) constant solid and fluid properties (thermophysical properties)
(6) negligible radiation of heat transfer,
(7) negligible superimposed natural convective heat transfer.

If the compressibility, the gravitational force and the dissipating heat caused by viscosity are neglected, the continuity, momentum ad energy equations for a fully developed 3D flow heat transfer are

3.5.1 Continuity Equation

$$\frac{\partial u}{\partial x} + \frac{\partial v}{\partial y} + \frac{\partial w}{\partial z} = 0 \tag{3.1}$$

3.5.2 Momentum Equation (Navier-stokes Equation)

X-momentum equation

$$\rho\left(u\frac{\partial u}{\partial x}+v\frac{\partial u}{\partial y}+w\frac{\partial u}{\partial z}\right)=-\frac{\partial p}{\partial x}+\mu\left(\frac{\partial^2 u}{\partial x^2}+\frac{\partial^2 u}{\partial y^2}+\frac{\partial^2 u}{\partial z^2}\right) \tag{3.2}$$

Y-momentum equation

$$\rho\left(u\frac{\partial v}{\partial x}+v\frac{\partial v}{\partial y}+w\frac{\partial v}{\partial z}\right)=-\frac{\partial p}{\partial y}+\mu\left(\frac{\partial^2 v}{\partial x^2}+\frac{\partial^2 v}{\partial y^2}+\frac{\partial^2 v}{\partial z^2}\right) \tag{3.3}$$

Z-momentum equation

$$\rho\left(u\frac{\partial w}{\partial x}+v\frac{\partial w}{\partial y}+w\frac{\partial w}{\partial z}\right)=-\frac{\partial p}{\partial z}+\mu\left(\frac{\partial^2 w}{\partial x^2}+\frac{\partial^2 w}{\partial y^2}+\frac{\partial^2 w}{\partial z^2}\right) \tag{3.4}$$

3.5.3 Energy Equation

$$\left(u \frac{\partial T}{\partial x} + v \frac{\partial T}{\partial y} + w \frac{\partial T}{\partial z} \right) = \frac{1}{\alpha} \left(\frac{\partial^2 T}{\partial x^2} + \frac{\partial^2 T}{\partial y^2} + \frac{\partial^2 T}{\partial z^2} \right) \tag{3.5}$$

3.6 Boundary Conditions

For a steady, fully developed laminar flow, $\frac{\partial u}{\partial x} = 0$, $v = 0$ and $w = 0$. If the whole unit cell is chosen as a unitary domain, the boundary conditions can be specified as follows.

3.6.1 Hydrodynamic Boundary Conditions

The velocity is zero at all boundaries except the channel inlet and outlet.

1. At the inner bottom wall surface of channel (no-slip condition)

$$u = 0 , \; v = 0, \; w = 0$$
$$\text{for } y = S_b \; , \; t < x < t + w \tag{3.6}$$

2. At inlet

$$p_1 = p_{in} \; , \; v = 0, \quad w = 0$$
$$\text{for } z = 0, \quad t < x < t + w \text{ and } S_b < y < S_b + h \tag{3.7}$$

3. At outlet

$$p_1 = p_{out}$$
$$\text{for } z = L \; , \; t < x < t + w \text{ and } S_b < y < S_b + h \tag{3.8}$$

3.6.2 Thermal Boundary Conditions

Adiabatic boundary conditions are applied to all the boundaries of the solid region except the heat sink bottom wall, where a constant heat flux is applied.

1. $-k_s \frac{\partial T}{\partial y} = q''$

   for $0 < z < L$, $0 < x < W$ and $y = 0$ (3.9)

2. At inlet, the liquid temperature is equal to a given constant inlet temperature.

   $$T = T_{in}$$

   for $z = 0$, $t < x < t + w$ and $S_b < y < S_b + h$ (3.10)

3. The flow is assumed to be thermally fully developed at the channel outlet.

   $$\frac{\partial^2 T}{\partial z^2} = 0$$

   for $z = L$, $t < x < t + w$ and $S_b < y < S_b + h$ (3.11)

The hydraulic diameter is calculated as below:

$$D_h = \frac{4A}{\Gamma} = \frac{4hw}{2(h+w)} \quad (3.12)$$

Fluid	ρ_f kg/m^3	k_f W/m-K	μ_f kg/m-s	c_p J/kg-K	T K
Water	998.2	0.6	0.001003	4182	293

Table 3.2 Thermophysical Properties of fluid.

Solid	ρ_s kg/m^3	k_s W/m-K	c_p J/kg-K
Silicon	2330	148	712

Table 3.3 Thermophysical Properties of solid.

Pressure	0.3
Density	1
Momentum	0.7
Body force	1

Table 3.4 Relaxation factors.

3.7 Closure

The total number of grid has taken is (20,0000 (i (x)× j (y) × k (z) =10 × 100 × 200) for the computational domain and shown in Fig. 3.3. The size of a fine grid mesh for the x and y directions was chosen in order to properly resolve the velocity and viscous shear layers as in Fig.3.4, and to more accurately define the conjugate heat transfer at the boundary layer of the channel, thereby improving the temperature result but along z-direction, comparative coarse discretization has been taken because the temperature gradients are small compared to the gradients occurring in other directions and process time as well as the memory storage required increases dramatically as the number of grid nodes is increased.

FLUENT's segregated solver has taken, which is an implicit solver. The unknown value for a given variable is computed from a set of linear equations, each of which is written for a single cell in the domain. Relaxation factors have direct impact on convergence. Generally default values are used, but if convergence problems occur, then these values are modified. Decreasing these factors gradually helps in convergence. Using segregated solver approach, the governing

equations are solved sequentially. Several methods like SIMPLE, SIMPLEC, SIMPLER and PISO are available for this purpose. For the present simulation the finite difference method and the SIMPLE algorithm are applied to solve the governing differential equations.

CHAPTER 4

Results and Discussions

- ***Introduction***
- ***Model Validation***
- ***Simulation of Single Microchannel***
- ***Closure***

4.1 Introduction

A three-dimensional model is developed to investigate flow and conjugate heat transfer in the microchannel based heat sink for electronic packaging applications. A series of numerical calculations have been conducted by FLUENT and the results are presented in order to show the effects of temperature distribution, heat flux distribution as well as the average heat transfer coefficient in the microchannel heat sinks.

The average of the area of microchannel has been taken for plotting the different gtaphs i.e average of the total number of nodes along the perimeter of the inner wall.

To better understand the fluid flow and heat transfer characteristics in silicon-based microchannel heat sinks designed for applications in electronic cooling. These non-circular channels and silicon base microchannel heat sinks combine the attributes of high material compatibility, high surface area per unit volume ratios and large potential heat transfer performance, with highly sophisticated and economic fabrication processes. These advantages make these silicon based microchannel heat sinks extremely attractive for a wide variety of commercial applications.

The different pressure drop, which are apply in FLUENT as shown in table 4.1.

Sink material	Δp (Pascal)
Silicon	10000
	20000
	35000
	50000
	65000

Table 4.1 Flow conditions for microchannel heat sink.

4.2 Model Validation

Model validation of the results of present study is done in two stages: grid independence test and results validation with previous numerical study works.

4.2.1 Grid Independence Test

The model is tested for grid-independence to give proper resolution to the region where large gradients of fluid flow and heat transfer characteristic is predicted. The optimum grid system has the meshing resolution as shown in Fig. 3.3 and 3.4. The model in this study uses a total number of grid 2,00000 (i (x)× j (y) × k (z) = 10 × 100 × 200). A grid independence test was carried out by doubling the grid size for the microchannel heat sink with the dimension given in table 3. 1.

The fine grid mesh for the x and y-directions is adopted to properly resolve the velocity and viscous shear layers and to more accurately define the conjugate heat transfer at the surface of the channel, thereby improving the temperature resolution. The meshing along the axial direction away from the entrance region a relatively coarse grid system has taken. The reasons for the comparative coarse discretization for the z-direction are, with the exception of the inlet region, the temperature gradients are small compared to the gradients occurring in other directions and the CPU time as well as the memory storage required increases dramatically as the number of grid nodes is increased. Furthermore comparison with standard numerical results, indicates that the finer the mesh size, the higher the numerical accuracy.

4.2.2 Model Validation with Previous Numerical Studies

The model of the present study is validated using average heat transfer coefficient inside the channel for constant pressure drop 50 kPa and heat flux 90 W/cm^2 as shown in Fig. 4.1. The result yield good agreement with the numerical results. It is significant that the present model demonstrates a better agreement with the numerical results in the average heat transfer coefficient compared to the model developed in Li's numerical work. The significant improvement of accuracy results given by the model in the present study is due to increase of density of grid system.

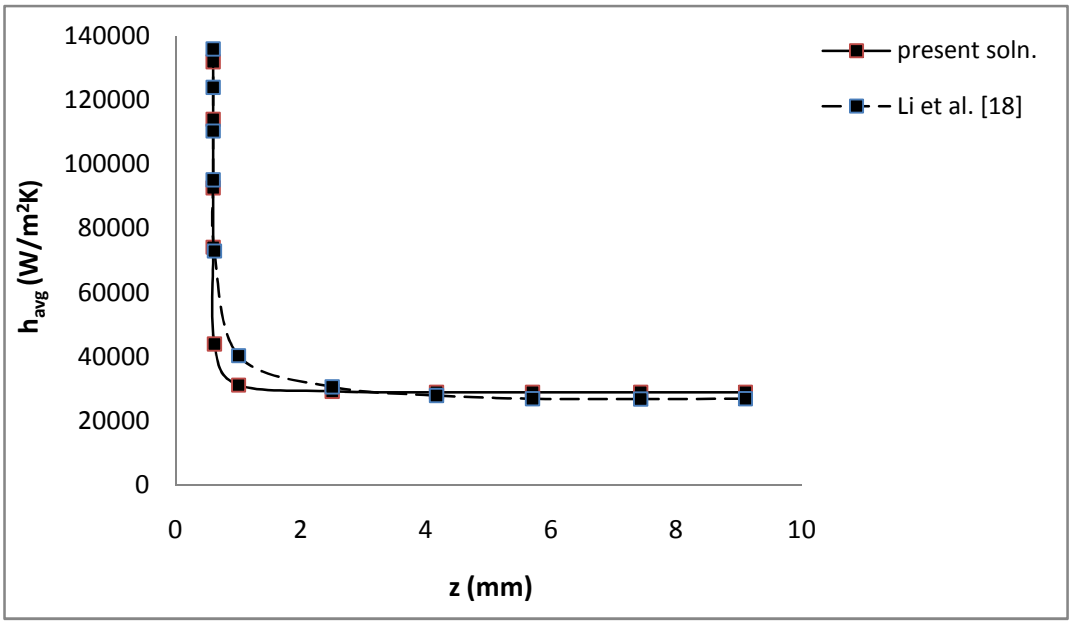

Fig. 4.1. Model validation using average heat transfer coefficient inside the channel with numerical result in *x*-*y* plane for $\Delta p = 50$ kPa at $q" = 90$ W/cm^2.

After setting the boundary conditions and flow conditions in microchannel geometry, iteration will be start. The model of the microchannel heat sink has been converged in 46 iteration. The simulation of convergence graph as shown in Fig. 4.2 below.

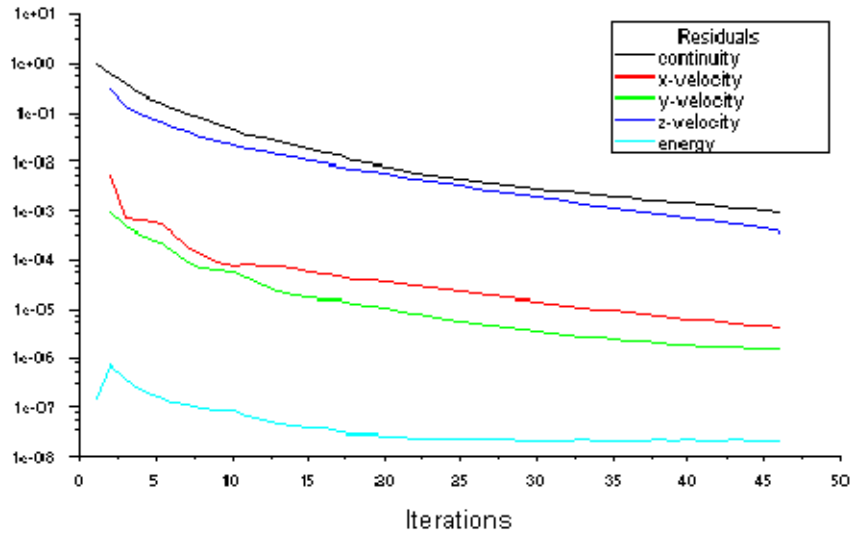

Fig. 4.2. Convergence graph.

4.3 Simulation of Single Microchannel

The single microchannel is simulated and the results of pressure contours, temperature contours, velocity vectors, average heat transfer coefficient, average Nusselt number variations along the flow direction and the effects of averaged heat flux at different walls of microchannel are presented. The variation of these parameters with a constant heat flux boundary is also discussed as follows.

4.3.1 Pressure Contours

The fluid is entered through the microchannel at pressure 50 kPa with constant inlet temperature 20 ^{o}C. After passing through the channel, the fluid discharged to the atmosphere i.e gauge pressure. A constant heat flux $q" = 90$ W/cm^2 is applied at the bottom wall of heat sink. The pressure contours inside channel as shown in Fig. 4.3.

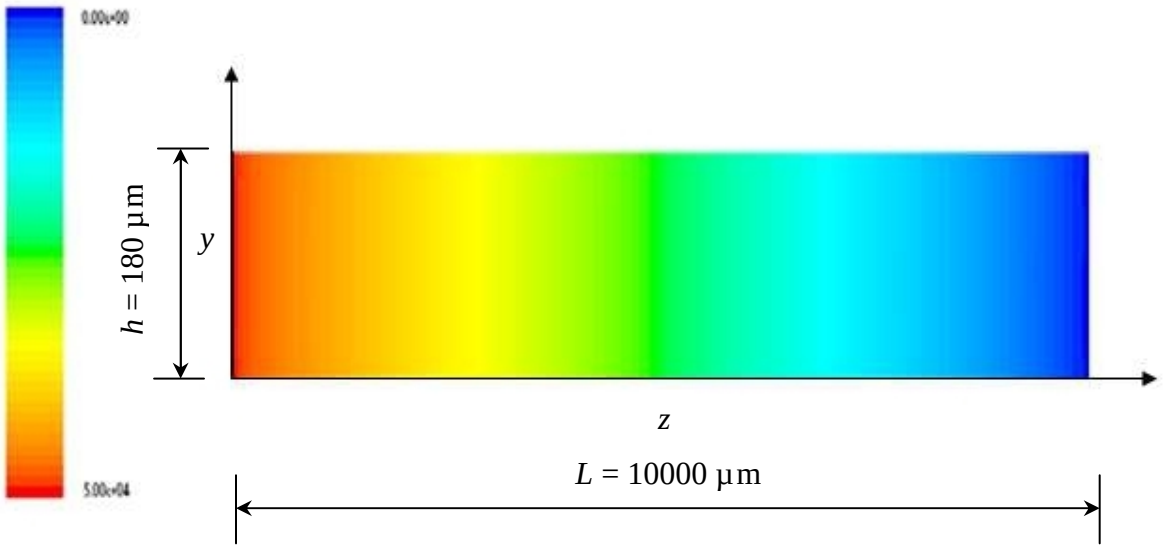

Fig. 4.3. Pressure contours of channel in *y*-*z* plane at x = 50 µm for Δp = 50 kPa and $q" = 90$ W/cm^2.

4.3.2 Temperature Contours

The temperature of fluid at the inlet is initially uniform (20 ^{o}C). The temperature Profiles shown is due to the assumption of hydrodynamic fully developed Flow. The temperature rise along the flow direction in the solid and fluid regions of the microchannel heat sink.

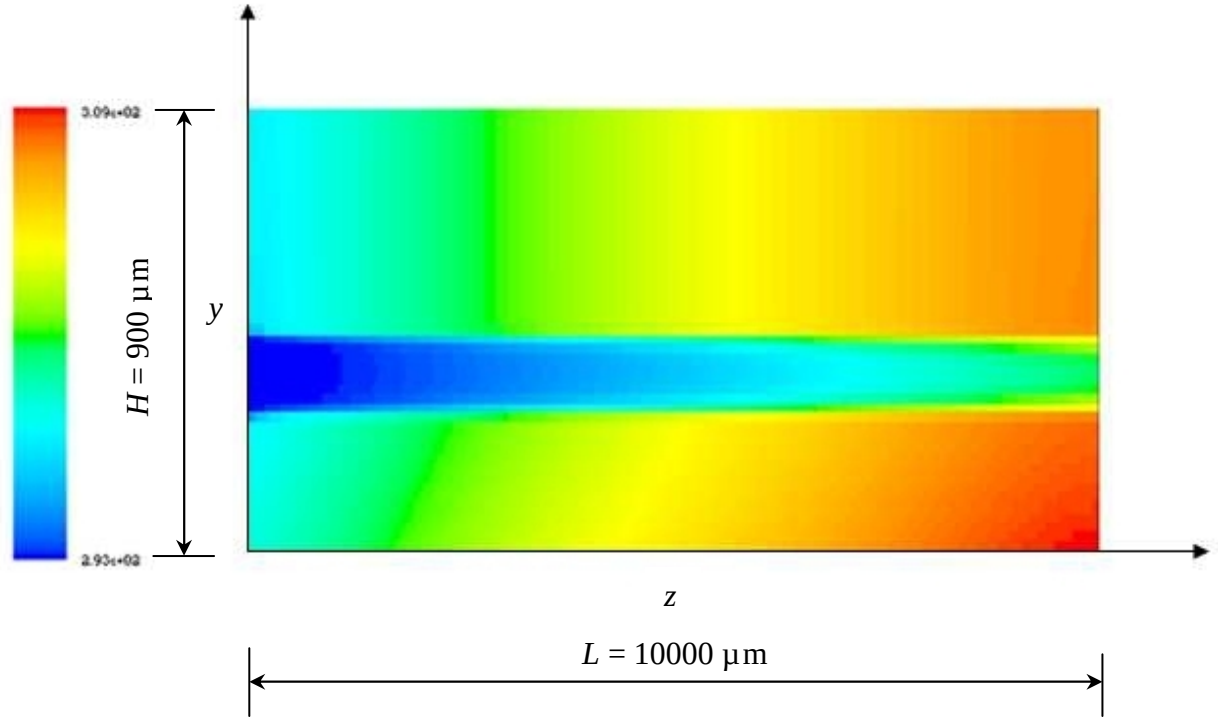

Fig. 4.4. Temperature contours in *y*-*z* plane at x = 50 µm for Δp = 50 kPa and q'' = 90 W/cm^2.

It is interesting to note that the temperature point is located at heated based surface of the heat sink as shown in Fig. 4.4, which is immediately below the channel outlet. This is due to the low velocity of the fluid flow and resulting high concentration of heat flux. Along the flow direction, the coolant temperature rises as the result of heat input; also it shows maximum temperature of fluid at exit of channel. Inside the channel, the fluid temperature rises from 20 ^{o}C to 36 ^{o}C. For prediction of fluid flow and thermal characteristics, contours of temperature in the fluid at the inlet and outlet of channel is shown in Fig. 4.5.

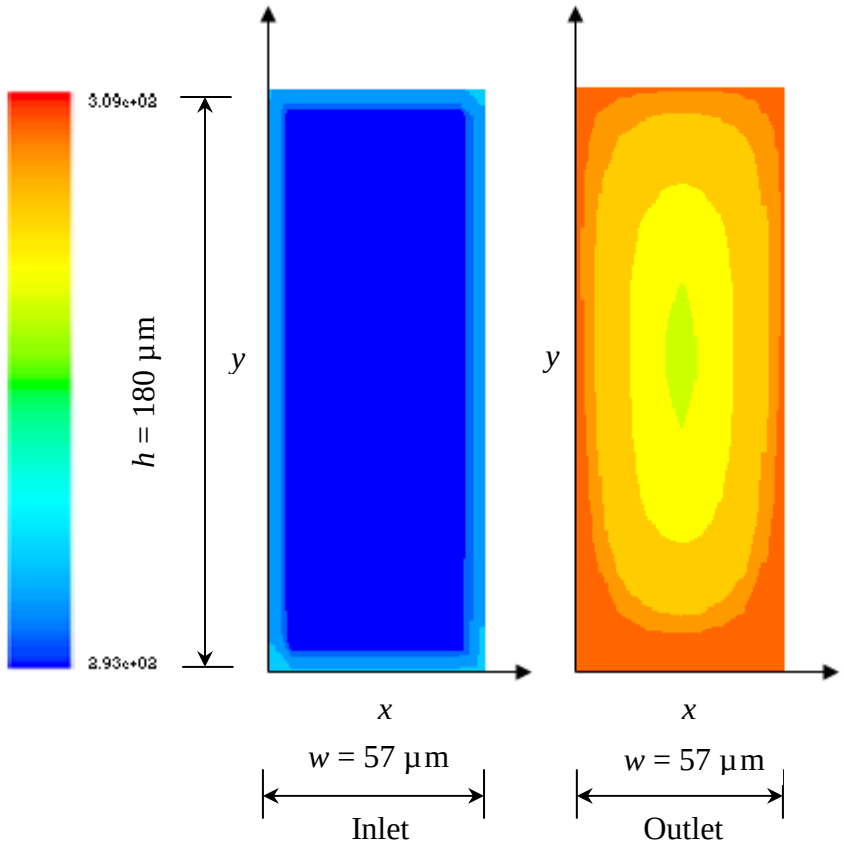

Fig. 4.5. Temperature contours of channel inlet and outlet in *x*-*y* plane at x = 57 µm for Δp = 50 kPa and q'' = 90 W/cm^2.

The principal issues in heat sink design are the overall heat transfer performance for electronic cooling and the local temperature gradient for determining the thermal stress. While a number of investigations are currently underway to actually measure the temperature and pressure gradients in these microchannels.

The highest temperature is obtained at the channel outlet in case of 10 kPa than 20 kPa and 50 kPa at constant heat flux of 90 W/cm^2 with inlet temperature 20 ^{o}C because of low velocity of fluid flow, the fluid get sufficient time to heat up as shown in Figs. 4.6, 4.7 and 4.8.

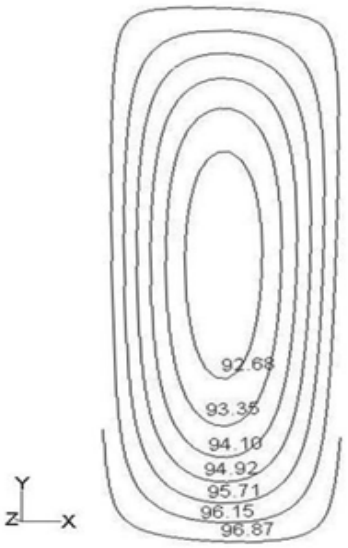

Fig. 4.6. Temperature contour inside the channel at the crossection of the outlet of the channel at outlet in *x*-*y* plane for Δp = 10 kPa and $q"$= 90 W/cm^2.

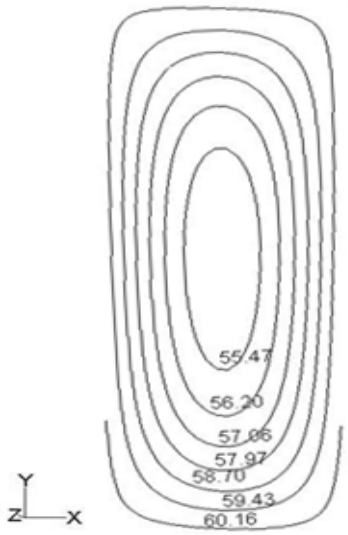

Fig. 4.7. Temperature contour inside the channel at the crossection of the outlet of the channel in *x*-*y* plane for Δp = 20 kPa and $q"$= 90 W/cm^2.

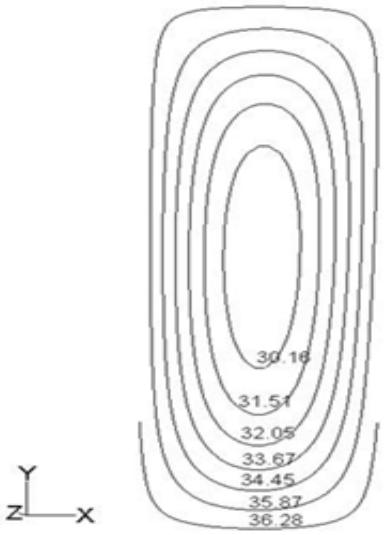

Fig. 4.8. Temperature contour inside the channel at the crossection of the outlet of the channel in *x*-*y* plane for $\Delta p = 50$ kPa and $q" = 90$ W/cm^2.

For further analysis, a constant pressure drop of 50 kPa and different heat flux of magnitude 50 W/cm^2, 90 W/cm^2 and 150 W/cm^2 has been taken in to consideration as shown in Figs. 4.9, 4.10 and 4.11. The highest temperature is obtained at the channel outlet in case of high heat flux i.e. 150 W/cm^2. As the heat flux increases, the outlet temperature goes on increasing because the fluid gets heated up more and more due to convective heat transfer, which is evident from the contours profiles.

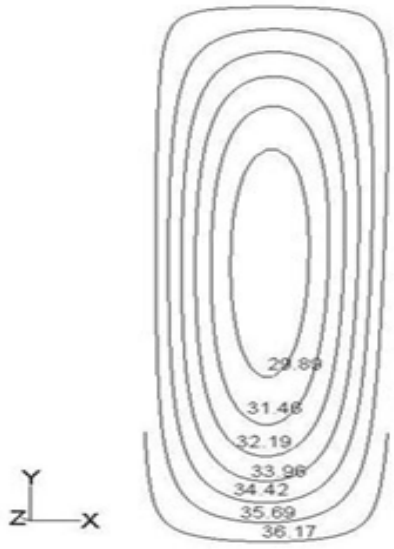

Fig. 4.9. Temperature contour inside the channel at the crossection of the outlet of th channel in *x-y* plane for $\Delta p = 50$ kPa and $q" = 50$ W/cm^2.

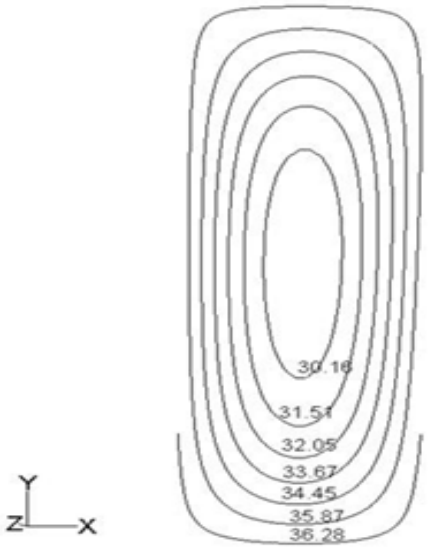

Fig. 4.10. Temperature contour inside the channel at the crossection of the outlet of the channel in *x-y* plane for $\Delta p = 50$ kPa and $q" = 90$W/cm^2.

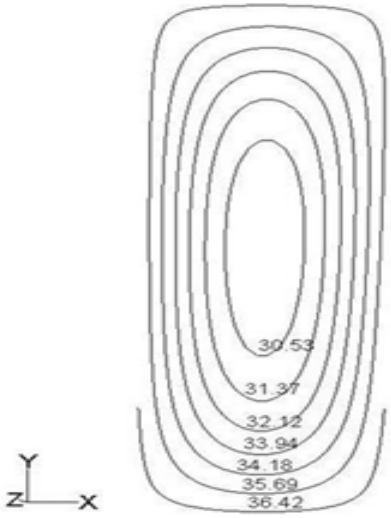

Fig. 4.11. Temperature contour inside the channel at the crossection of the outlet of the channel in *x*-*y* plane for Δp = 50 kPa and q'' = 150 W/cm^2.

The fluid is entering through the channel at temperature 20 ^{o}C at constant pressure drop 50 kPa and then temperature goes on increasing up to 36 ^{o}C due to continuous supply of heat flux q'' = 90 W/cm^2. From the Fig. 4.12, it is clear that highest temperature is encountered at the channel outlet.

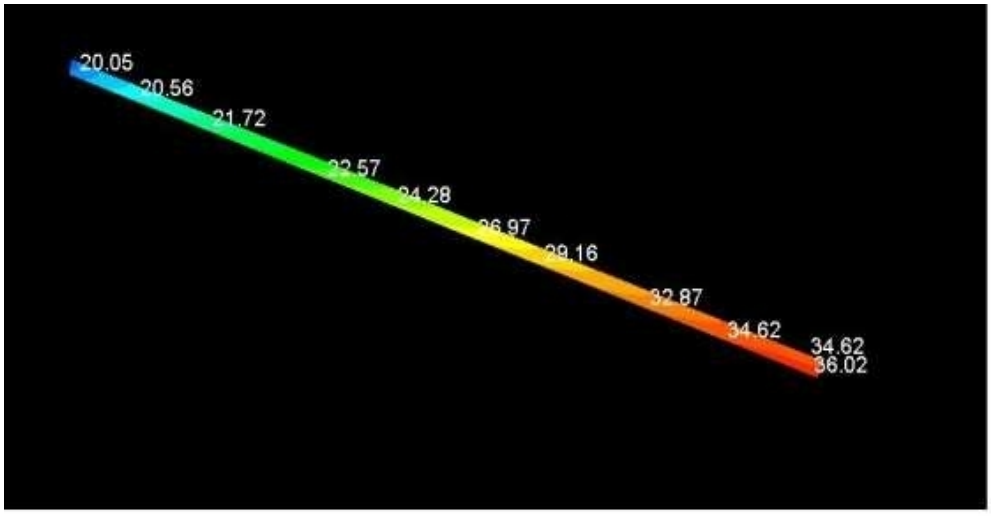

Fig. 4.12. Liquid temperature distributions inside the channel in *x*-*y* plane for Δp = 50 kPa and q'' = 90 W/cm^2.

Inside the microchannel the temperature of fluid rises up to 62 ^{o}C in case of 10 kPa due to low liquid velocity, a large portion of the heat is conducted in to the front part of the heat sink and in case of 50 kPa, the temperature rises up to 36 ^{o}C, due to high liquid velocity, a small portion of heat is conducted in to the front part of the heat sink at constant inlet temperature 20 ^{o}C as shown in Fig. 4.13.The liquid temperature variations for different pressure drop at constant heat flux as shown in Table 4.2.

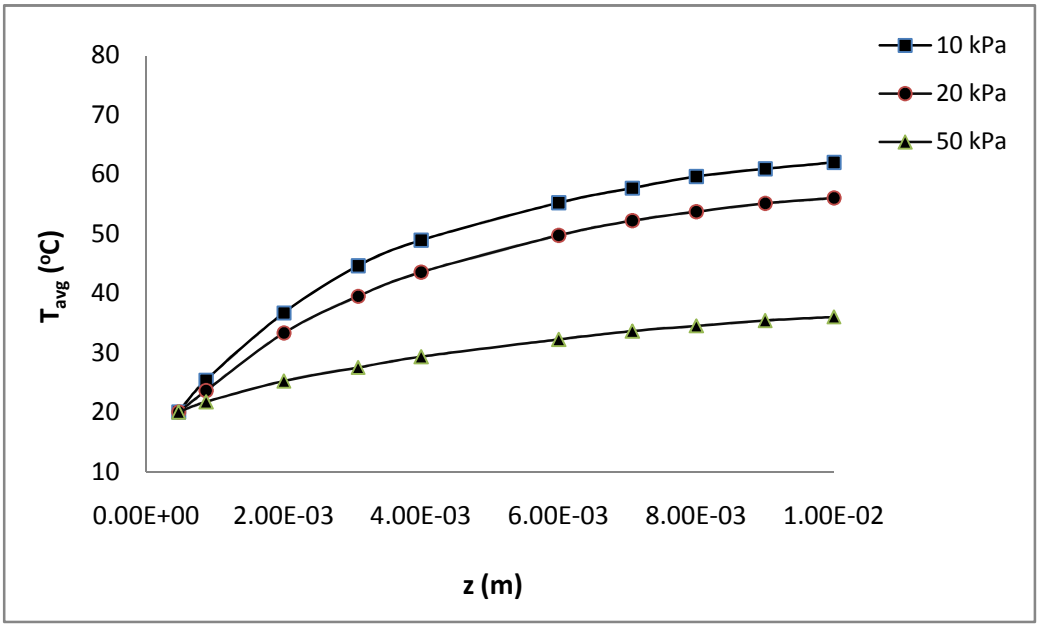

Fig. 4.13. Average liquid temperature variations inside the channel in *x-y* plane for different pressure drops and $q" = 90$ W/cm^2.

Δp (Pascal)	Inlet temperature (^{o}C)	Outlet temperature (^{o}C)
10000	20	62
20000	20	56
35000	20	46
50000	20	36
65000	20	26

Table 4.2 Inlet and outlet temperature of liquid for different pressure drop.

4.3.3 Velocity Vectors

The maximum velocity is obtained at the side of the channel outlet and minimum velocity is found at the center. Velocity vectors at outlet of channel for pressure difference of 50 kPa and heat flux of 90 W/cm^2 shown in Fig. 4.14.

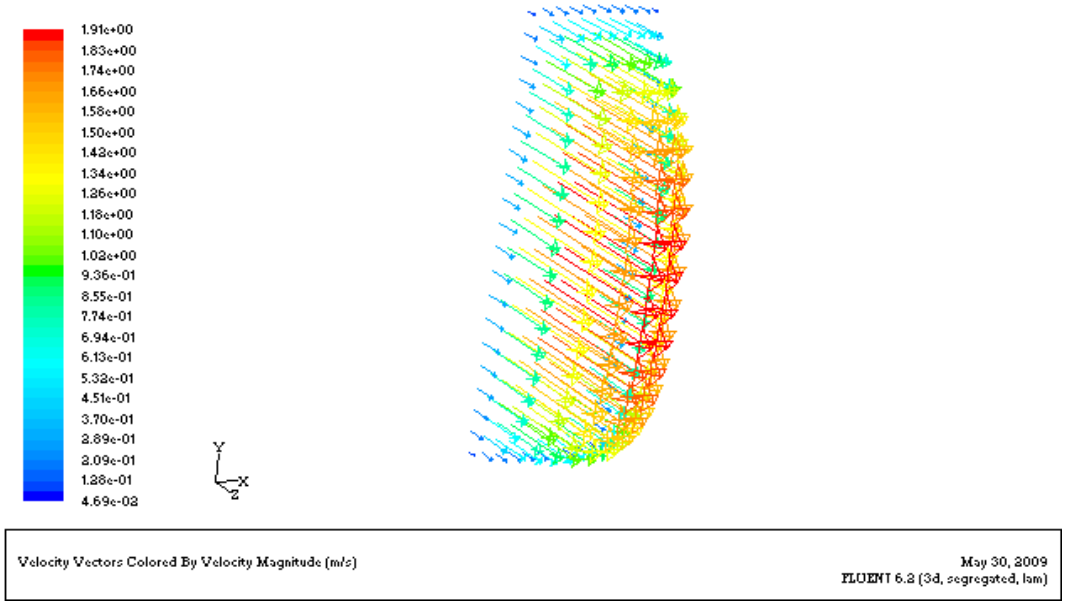

Fig. 4.14. Velocity vectors at outlet of channel in *x*-*y* plane at $x = 57\mu m$ for $\Delta p = 50$ kPa and $q'' = 90$ W/cm^2.

4.3.4 Average Heat Transfer Coefficient

The average heat transfer coefficient sharply decreases at 1/10th of microchannel as shown in Fig. 4.15. For this the temperature of water is also found less at the entrance region and more at the exit of the channel.

Due to growing boundary layer thickness, the heat transfer coefficient decreases along the flow direction and it is extremely high in the entrance region due to very thin local boundary layer. It decreases asymptotically to the fully developed value if the channel is sufficient long. The average heat transfer coefficient is simply defined as $h_{avg} = \frac{q''}{\Delta T_{avg}}$, which is determined based upon the heat flux density applied to the bottom of the substrate and the temperature

difference between the average substrate wall temperature and the bulk liquid temperature $\left(\Delta T_{avg} = T_w - T_f\right)$.

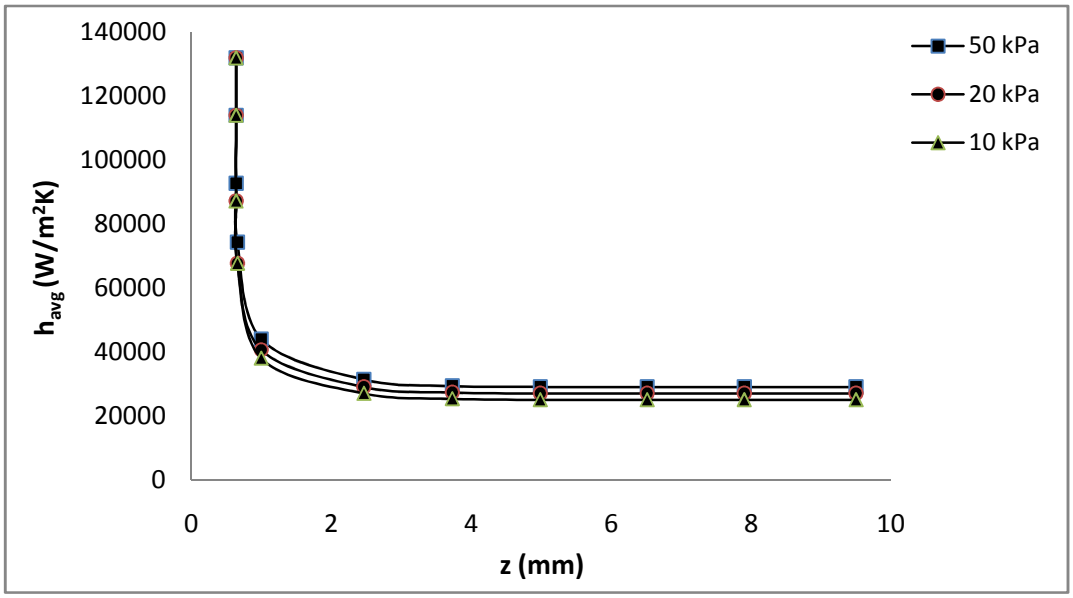

Fig. 4.15. Average heat transfer coefficient distributions inside the channel in *x*-*y* plane for different pressure drop at $q" = 90$ W/cm^2.

4.3.5 Average Nusselt number

The average Nusselt number 4.1 obtained in case of $\Delta p = 50$ kPa, lies between the values for a constant axial wall heat flux 4.8 and a constant axial wall temperature 4.0, for fully developed laminar flow in ducts, of rectangular cross-section with approximately [*w*: *h* = 1: 3 (57:180)]. It should be approximately 4.0 because of the limitations in the grid size used in the simulation. The average Nusselt number decreases along the channel due to formation of boundary layer and it is extremely high in the entrance region for different pressure drops (50, 20 and 10 kPa) due to very thin boundary layer as shown in Fig. 4.16. The average Nusselt number is simply defined as $Nu = \frac{h.D_h}{k_f}$ .The output results of average Nusselt number is compared with numerical results of Li [18] as shown in Fig. 4.17.

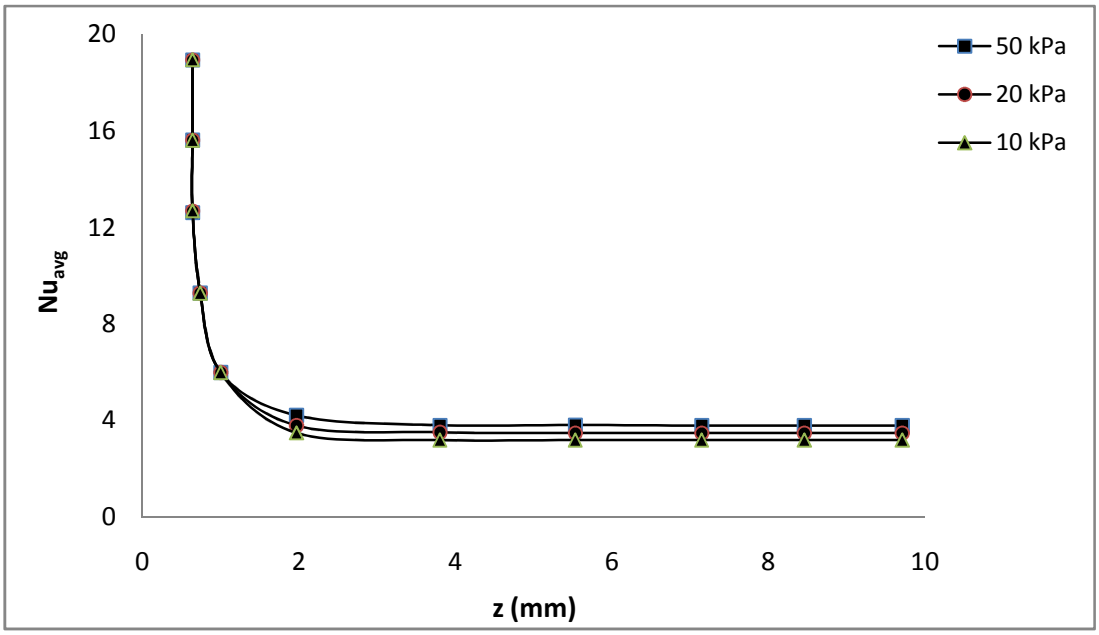

Fig. 4.16. Average Nusselt number distributions inside the channel in *x*-*y* plane for different pressure drop at $q"= 90$ W/cm^2.

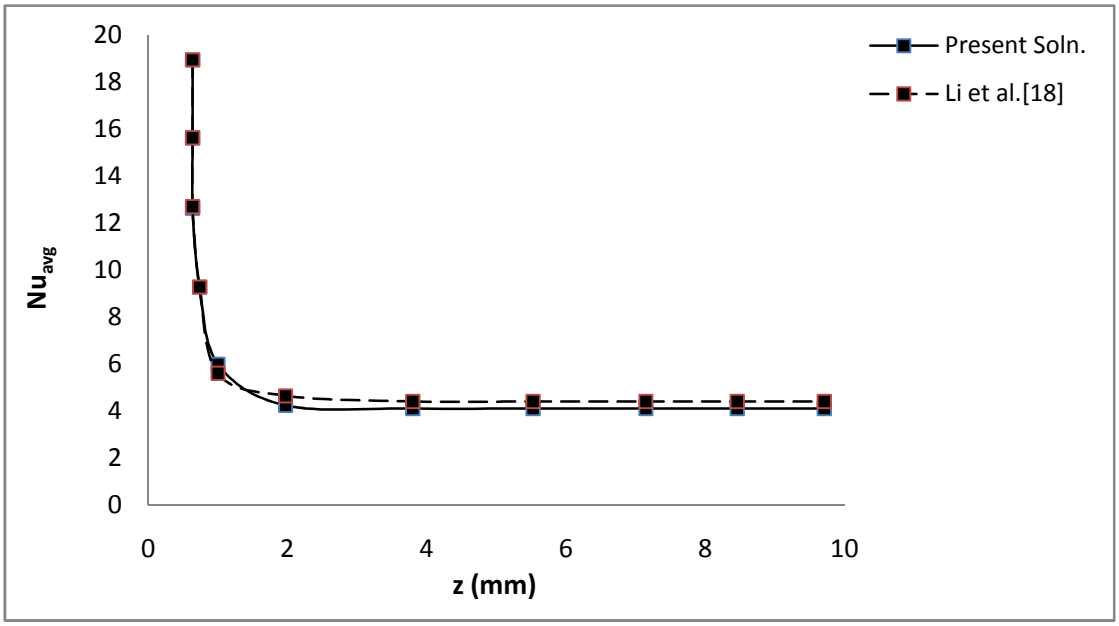

Fig. 4.17. Comparison between the FLUENT results and numerical results for average Nusselt number in *x*-*y* plane for $\Delta p = 50$ kPa at $q"= 90$ W/cm^2. [63]

4.3.6 Heat Transfer Coefficient Variations for Different Heat Flux

As the heat flux increases the average heat transfer coefficient increases along the channel length because of growing boundary layer thickness and it increases in the entrance portion due to thin boundary layer for different heat flux of magnitude 50 W/cm^2, 90 W/cm^2 and 150 W/cm^2 as shown in Fig. 4.18.

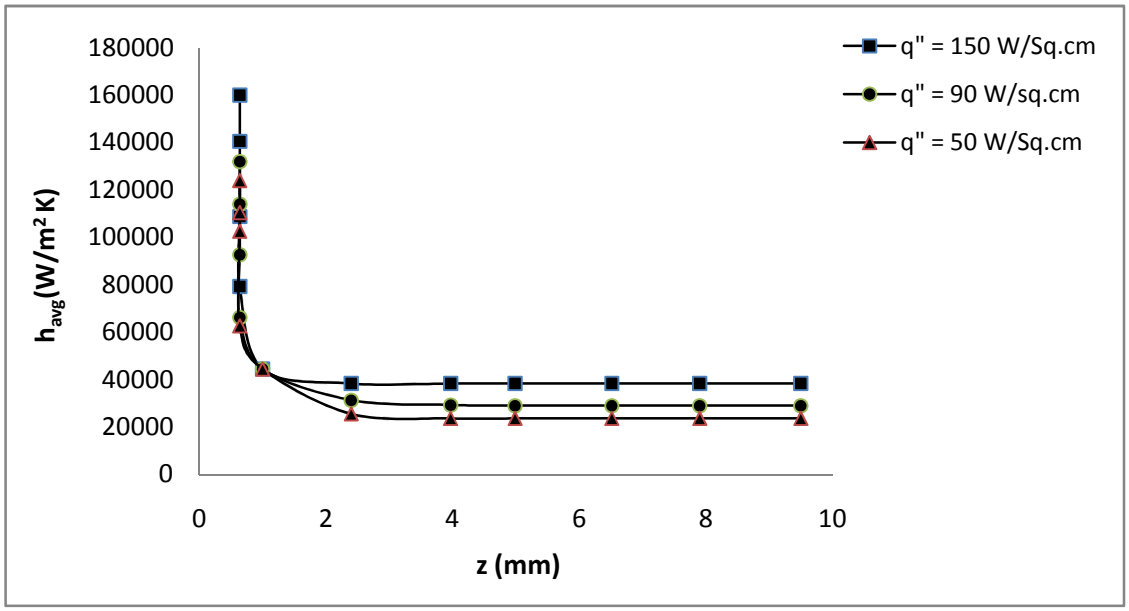

Fig. 4.18. Axial variations of average heat transfer coefficient in *x*-*y* plane for different heat fluxes at Δp = 50 kPa.

4.3.7 Nusselt number Variations for Different Heat Flux

The average Nusselt number increases with increase in heat flux along the channel length for different heat flux of magnitude 150, 90 and 50 W/cm^2. It decreases along the flow direction due to growing boundary layer thickness and it increases at inlet due to thin boundary layer as shown in Fig. 4.19.

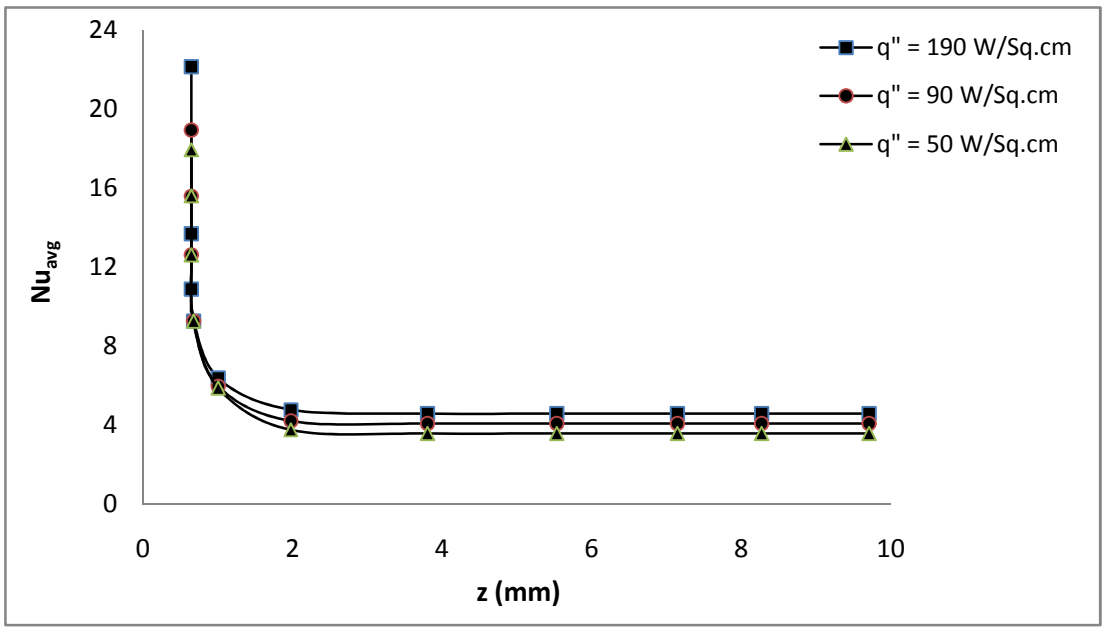

Fig. 4.19. Axial variations of average Nusselt number in *x*-*y* plane for different heat fluxes at Δp = 50 kPa.

4.3.8 Heat Flux Distribution

High heat flux is found in the region near the channel inlet. This is due to the thin thermal boundary layer in the developing region and gradually it decreases along the flow direction because of growing boundary layer thickness. The heat flux varies around the channel periphery, approaching zero in the corners where the flow is generally weak for a rectangular channel. Figs. 4.20, 4.21 and 4.22 shows that increasing the pressure drop increased the heat flux flow at top, bottom and side wall significantly.

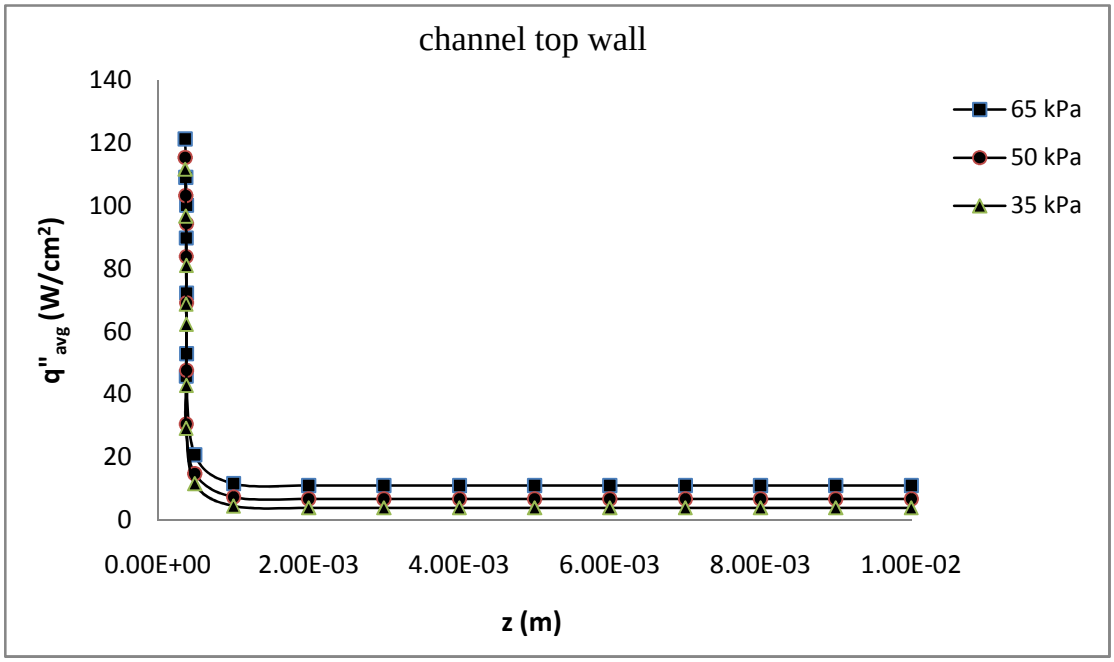

Fig. 4.20. Average heat flux distributions at top walls along the channel length in *x*-*y* plane for Δp = 65, 50 and 35 kPa at $q"$ = 90 W/cm^2.

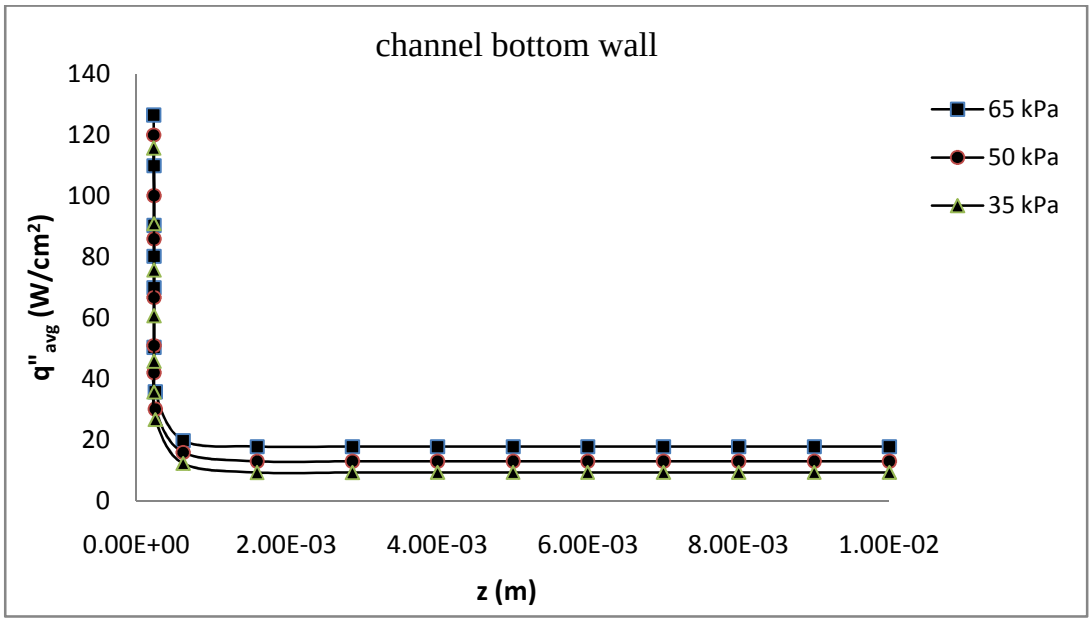

Fig. 4.21. Average heat flux distributions at bottom walls along the channel length in *x*-*y* plane for Δp = 65, 50 and 35 kPa at $q"$ = 90 W/cm^2.

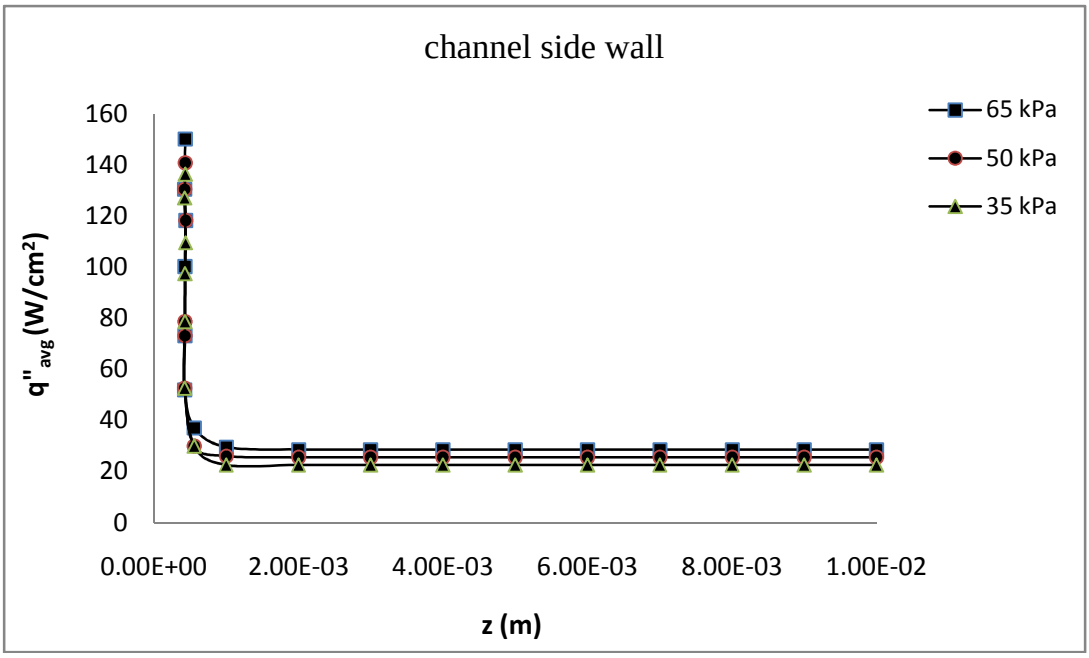

Fig. 4.22. Average heat flux distributions at side walls along the channel length in *x*-*y* plane Δp = 65, 50, 35 kPa at $q"$= 90 W/cm^2.

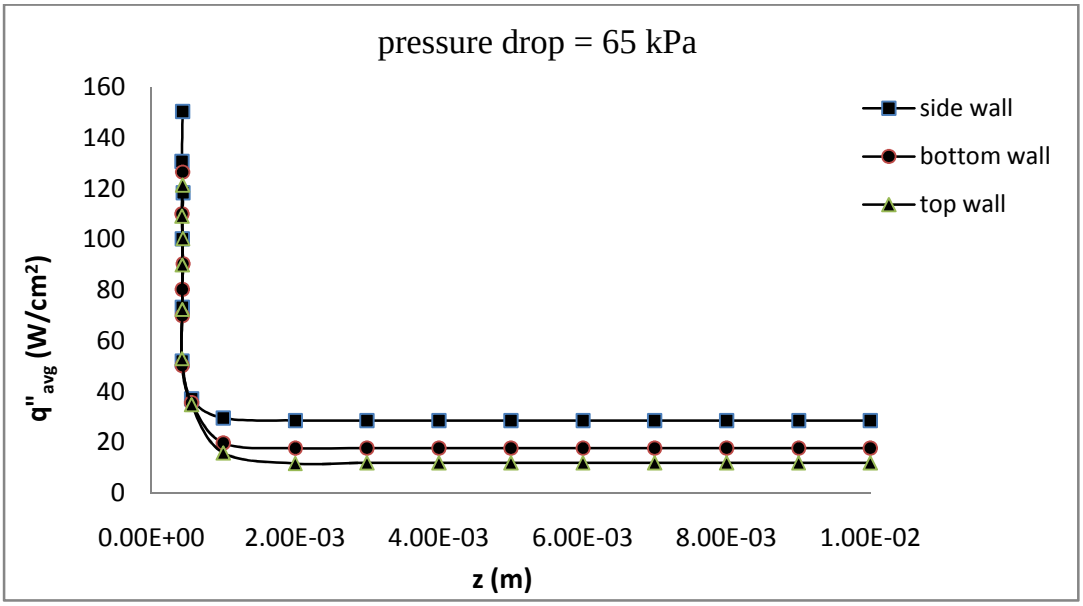

Fig. 4.23. Average heat flux distributions at side, bottom and top walls along channel length in *x*-*y* plane for Δp = 65 kPa at $q"$= 90 W/cm^2.

The heat flux at the channel bottom wall as shown in Fig. 4.21 is only slightly larger than at the top wall in Fig. 4.20. This implies that although the heat is supplied to the heat sink bottom wall, it is spread out very effectively with in the solid region by conduction. So the heat flux at the channel side wall is higher than that the channel bottom and top walls due to short distance between the solid walls and the large velocity gradient present as shown in Fig. 4.23.

4.4 Closure

An investigation of the fluid flow and heat transfer phenomena in microchannel heat exchangers was conducted. A review of the literature published on research conducted in microchannel fluid flow and heat transfer over the two decades was completed. An analysis of some of the methods of experimentation and data reduction found in the literature was performed, and it was found that major obstacles in implementing this technology are due to the lack of substantial understanding in the behavior of microchannel system. In reality, it is difficult to achieve an adiabatic boundary at the inlet and outlet of the heat sink as assumed in the numerical model, a significant portion of the heat loss is transferred to the ambient environment, especially for low fluid flow conditions. One drawback of microchannel heat ink is the relatively higher temperature rise along the microchannels compared to that for the traditional heat sink designs. The large amount of heat generated by semiconductor chips is carried out from the package by a relatively small amount of coolant, so the coolant exists at a relatively high temperature. This undesirable high temperature gradient is an important consideration in the design of an electronic cooling scheme. The maximum temperature is found at the channel outlet in case of low pressure drop and high heat flux. As the boundary layer thickness is small at the entrance portion, the heat transfer coefficient, Nusselt number and heat flux is extremely high in that portion but these perimeters are gradually decreases along the flow direction due to growing boundary layer thickness. As the heat flux is supplied at the channel bottom wall but side wall exhibit more heat than top and bottom wall due to conduction.

CHAPTER 5

Conclusions and Further work

- ***Conclusions***
- ***Suggestions for Further work***

5.1 Conclusions

The theoretical analysis performed, provides a fundamental understanding of the combined flow and conjugate convection-conduction heat transfer in the three-dimensional microchannel heat sink. The model formulation is general and only a few simplifying assumptions are made. Therefore, the results of the analysis as well as the conclusions can be considered as quite general and applicable to any three-dimensional conjugate heat transfer problem.

- A three-dimensional rectangular microchannel model consists of a 10 mm long silicon substrate with 57 µm wide and 180 µm deep developed using incompressible laminar Navier-Stokes equations of motion is capable of predicting correctly the flow and conjugate heat transfer in the microchannel heat sink. It has been validated using numerical data reported in the literature and a good agreement has been found between the model prediction and measurements.

- The combined conduction–convection heat transfer in the microchannel produces very complex three-dimensional heat flow pattern with large, longitudinal, upstream directed heat recirculation zones in the highly conducting silicon substrate, where the fluid and solid are in direct contact. A detailed description of the average heat transfer coefficient, temperature, heat flux and Nusselt number was obtained. General conclusions that stemmed from this analysis are presented, together with a brief recapitulation of some of the important remarks made earlier.

- The maximum temperature is located at heated base surface of heat sink, below the channel outlet. This is due to the low velocity of the fluid flow and resulting high concentration of heat flux.

- The highest temperature is obtained at the channel outlet in case of 10 kPa at constant heat flux of 90 W/cm^2, because of low velocity of fluid flow. At heat flux $q" = 150$ W/cm^2 the highest temperature is obtained at the channel outlet at constant pressure drop of 50 kPa. As the heat flux increases, the outlet temperature goes on increasing because the fluid gets heated up more and more due to convective heat transfer. The maximum temperature of fluid rises in case of 10 kPa due to low liquid velocity and minimum temperature rises in case of 50 kPa due to high liquid velocity inside the microchannel at constant inlet temperature 20 ^{o}C.

- The variations of the heat transfer coefficient and the Nusselt number along the flow direction is quite small for this type of microchannel heat sink after the thermal entrance lengths. It should be noted that since the grid size in the flow direction is relatively coarse, the heat transfer is not as accurate as the case for the *x* and *y*-direction. However the resolution is sufficient to aid in the design of micro-heat sinks for industrial applications and also to provide information and insight in to the fluid flow characteristics in the flow direction.

- The average heat transfer coefficient, average Nusselt number variations decreases along the flow direction due to growing boundary layer thickness and extremely high at the entrance region due to the very thin local boundary layer. As the heat flux increase, the average heat transfer coefficient and average Nusselt number also increases for constant pressure drop.

- The average heat fluxes from the solid to the coolant in the small inlet region of the microchannel are larger than those in the further downstream portion. This is because the average convective heat transfer coefficient is much larger in the upstream locations (the boundary layer thickness is small) and also because the highly conducting channel walls support very effective heat redistribution from the downstream (large convective resistance) to the upstream (small convective resistance) regions of the channel. This finding supports the concept of the MMC heat sink where the flow length is greatly reduced to small fraction of the total length of the heat sink [70,71] by using a design with multiple inter connected inlets and outlets.

- The heat flux at the channel side wall is higher than the channel bottom and top walls due to short distance between the solid walls and the large velocity gradient present.

- The present analysis and experimental data strongly indicate that the forced convection water cooled microchannel heat sink has a superior potential for application in thermal management of the electronic packages. The heat sink is compact and is capable of dissipating a significant thermal load (heat fluxes of the order of 90 W/cm^2) with a relatively small increase in the package temperature (less than 20 ^oC).

5.2 Suggestions for Further Work

From the investigation of single microchannel heat fluid flow analysis, it is found that sometimes the temperature of fluid will be very high i.e. above the boiling temperature of fluid. In that case a multiphase flow analysis may be treated to predict the microchannel performance. The positioning of the microchannel for maximum heat pumping capability on the sink material is also an interest of study.

In the one-layered microchannel heat sink design, fluid temperature rise along the flow direction in both the solid and cooling fluid. The temperature rise produces thermal stresses in chips and packages due to the coefficient of thermal expansion mismatch among different materials thus undermining device reliability. Therefore more sophisticated predictions of the temperature field are essential for an effective microchannel heat sink design. Also it can be controlled by increasing the pressure drop across the channel. A larger pressure drop forces coolant to move faster through the channel, thereby, requiring more powerful pumping power supply, generating more noise and requiring bulkier packaging.

Two phase microchannel heat sink is an alternative method for eliminating the temperature variations, in which the utilization of latent heat can achieve a uniform temperature profile on the heating surface.

Further work may include the influence temperature-dependency of material thermophysical properties other than viscosity such as density and specific heat. The effect of pollutants and impurities in the microchannel heat sink material may also be considered. This may help us to better understand potential regions of thermal stress and hot spots in microchannel heat sink design.

APPENDIX

In CFD calculations, there are three main steps.

1) Pre-Processing
2) Solver Execution
3) Post-Processing

Pre-Processing is the step where the modeling goals are determined and computational grid is created. In the second step numerical models and boundary conditions are set to start up the solver. Solver runs until the convergence is reached. When solver is terminated, the results are examined which is the post-processing part.

Steps in GAMBIT and FLUENT for solving 3-Dimensional Microchannel Heat Sink problem

1. Steps (3-D Version of GAMBIT)

STEP 1: Specify that the mesh to be created is for use with FLUENT 6.0:

Main Menu > Solver > FLUENT 5/6
Verify this has been done by looking in the *Transcript Window* where you should see. The boundary types that you will be able to select in the third step depends on the solver selected.

STEP 2: Creation of vertices

Operation>Geometry>Vertex >Create real Vertex from Co-ordinates**.**
The following vertices with the required Cartesian co-ordinates were created. All dimensions are in 'µm'

x	y
0	0
100	0
100	270
100	450
100	900
100	900
0	450
0	270
21.5	270
78.5	270
78.5	450
21.5	450

STEP 3: Creation of line

Operation>Geometry>Creating Straight edge
Create straight edge by joining the following vertices
AB, BC, CD, DE, EF, FG, GH, HA, IJ, JK, KL, LI, GL, HI, JC and KD.

STEP 4: Creation of Faces

Operation>Geometry>Face > Create Face from Wireframe
To create face 'ABCJIH', select edges in a sequence order (AB>BC>CJ>JI>IH>HA) and click apply
Similarly create faces CDKJC, IKLIJ, LGHIL, DEFGLKD and apply the same above commands.

STEP 5: Meshing Edges

Operation>Mesh>Edge>Mesh Edges

(a) Select edges LK and IJ
Type Successive ratio
Click Double sided
Ratio 1 - 1.1, Ratio 2 - 1.1
Spacing - apply
Interval count - 10
Mesh - apply

(b) Select edges LI and KJ
Type Successive ratio
Click Double sided
Ratio 1 - 1.2, Ratio 2 - 1.2

Spacing - apply
Interval count - 20
Option - Mesh and apply

STEP 6: Meshing Faces (front side of channel face)

(a) Operation>Mesh>Face>Mesh Faces
Select face - IJKL
Elements - Quad
Type - Map
Spacing - not apply
Option - Mesh and apply

STEP 7: Meshing Faces (except channel)

(a) Operation>Mesh>Face>Mesh Faces
Select face - GHIL and CDKJ
Elements - Quad
Type - Map
Spacing - apply
Interval count - 20
Option - Mesh and apply

(b) Select face - DEFGLK
Elements - Quad/Tri
Type - Pave
Spacing - not apply
Interval size - 10
Option - Mesh and apply

(c) Select face - ABCJIH
Apply the same procedure mentioned above.

STEP 8: Creation of Volume

Operation>Geometry>Volume>Sweep faces
Faces - Select all faces
Path - Vector, Define
Direction - Z - positive
Magnitude - 10000 and apply
Apply

STEP 9: Create Mesh Face (back side of heat sink face)

Operation>Geometry>Face>Move/Copy Faces

Select faces - All mesh faces
Copy
Local - z - 10000
Copy mesh linked and Apply

STEP 10: Creating of Mesh Volume

Operation>Mesh>Volume>Mesh Volumes
Volumes - Select all volumes
Elements - Hex/Wedge
Type - Cooper
Spacing - Apply
Interval count - 50
Option - Mesh and Apply

STEP 11: Creating of Zones

Operation>Zones>Specify Boundary Types
Entity - Face

Label	Name	Type	Click
Channel inlet	Pressure inlet	Pressure inlet	Apply
Channel outlet	Pressure outlet	Pressure outlet	Apply
Sink top	Insulated top	Wall	Apply
Sink bottom	Heat flux	Wall	Apply
Sink left side	Insulated left	Wall	Apply
Sink right side	Insulated right	Wall	Apply
Channel top	Coupled top	Wall	Apply
Channel bottom	Coupled bottom	Wall	Apply
Channel left side	Coupled left	Wall	Apply
Channel right side	Coupled right	Wall	Apply

STEP 12: Creation of Continuum

Operation>Zones>Specify Continuum Types

Entity - Volumes

Label	Name	Type	Click
Heat sink	Sink	Solid	Apply
Channel	Water	Fluid	Apply

STEP 13: File>Save as>Browse>Filter [File Name]>Selection[Same Name]>Accept>Accept

STEP 14: Export>Mesh>Browse>Filter [File Name]>Selection[Same Name]>Accept>Accept

STEP 15: File>Exit>Yes

2. Steps (3-D Version of FLUENT)

STEP 16: Select FLUENT

Version>3d>Run

STEP 17: Read Mesh File

File>Read>Case

Select mesh file from destination folder

STEP 18: Grid>Check

It was checked that the total volume doesn't come as negative

STEP 19: Grid>Info>Size

It shows the cells, faces and nodes

STEP 20: Grid>Scale

Unit conversion[Grid was created in mm]>Scale>Scale[To convert it in to 'm']

STEP 21: Grid>Smooth/Swap

The grid was swapped until Zero faces were moved

STEP 22: Define>Models>Solver

Solver: Segregated

Formulation: Implicit

Space: 3 D

Time: Steady, Ok

STEP 23: Define>Models>Viscous

Model: Laminar, Ok

STEP 24: Define>Models>Energy

Energy: Energy equation

STEP 25: Define>Materials

Material type: Solid

Fluent Database: Select Silicon material

Properties: Density(kg/m^3) - 2330

Specific Heat Capacity(J/kg-K) - 712

Thermal conductivity(W/m-K) - 148

Material type: Fluid

Fluent Database: Select water - liquid

Properties: Density(kg/m^3) - 998.2

Specific Heat Capacity(J/kg-K) - 4182

Thermal conductivity(W/m-K) - 0.6

Viscisity(kg/m-s) - 0.001003

STEP 26: Define>Operating conditions

Gravity: Gravitational Acceleration)

Direction: y = - 9.81m/s^2

Operating Temperature(K) – 293

STEP 27: Define>Boundary conditions

(a) Zone: Pressure inlet

Type: Pressure inlet

Set: Gauge total pressure(Pascal) - 50000

Total temperature(K) - 293

X - component flow direction - 1

Y - component flow direction - 0

Z - component flow direction - 1, Ok

(b) Zone: Heat flux

Type: Wall

Set: Thermal condition - Heat flux

Heat flux(W/m^2) - 900000, Ok

(c) Zone: Sink wall

Set: Thermal condition - Heat flux

Heat flux(W/m^2) - 0, Ok

(d) Zone: Water

Set: Material name - Water - liquid, Ok

STEP 28: Solve>Controls>Solutions

Equations: Flow and energy equations used

Pressure-Velocity Coupling - SIMPLE

Under relaxation factors: Pressure - 0.3

Density - 1

Body Force - 1

Momentum - 0.7

Energy - 1

Discretization: Pressure = Second order

Momentum = Second order upwind

Energy = Second order upwind

STEP 29: Solve>Initialize>Initialize

Compute from: Heat flux

Initial values: X - velocity(m/s) - 0

Y - velocity(m/s) - 1

Z - velocity(m/s) - 1, Init, Apply, Close

STEP 30: Solve>Monitors> Residual

Option: Print>Plot

Plotting: Window - 1 Iterations - 1000

Residual: Convergence criterion

Continuity - 0.001

X - velocity = 0.001

Y - velocity = 0.001

Z - velocity= 0.001

Energy= 1e-06

STEP 31: Solve>Iterate

No. of iterations =100.

Iterate - till the solution is converged

REFERENCES

1. Hetsroni, G., Mosyak, A. and Segal, Z., (2001), "Non-uniform temperature distribution in electronic devices cooled by flow in parallel microchannels", *IEEE Transactions on Components and Packaging Technologies*, Vol. 24, pp. 16-23.

2. Hetsroni, G., Mosyak, A., Segal, Z. and Pogrebnyak, E., (2003), "Two-phase flow patterns in parallel microchannels", *International Journal of Multiphase Flow*, Vol. 11, pp. 353-358.

3. Bau, H.H., (1998), "Optimization of conduits' shape in micro heat exchangers", *International Journal of Heat and Mass Transfer*, Vol. 41, pp. 2717-2723.

4. Culham, J.R., Yovanovich, M.M. and Lemczyk, T.F., (2000), "Thermal characterization of electronic packages using a three-dimensional fourier series solution", *ASME Journal of Electronic Packaging*, Vol. 122, pp. 233-239.

5. Davies, M.R.D., Cole, R. and Lohan, J., (2000), "Factors affecting the operational thermal resistance of electronic components", *ASME Journal of Electronic Packaging*, Vol. 122, pp. 185-191.

6. Pucha, R.V., Tunga, K., Pyland, J. and Sitaraman, S.K., (2004), "Accelerated thermal guidelines for electronic packages in military avionics thermal environment", *ASME Journal of Electronic Packaging*, Vol. 126, pp. 256-264.

7. Zhao, C.Y. and Lu, T.J., (2002), "Analysis of microchannel heat sinks for electronics cooling", *International Journal of Heat and Mass Transfer*, Vol. 45, pp. 4857-4869.

8. Chen, Han-Ting., Jenn-Tsong, Horng., Chen, Po-Li. and Hung, Ying-Huei., (2004), "Optimal design for PPF heat sinks in electronics cooling applications", *ASME Journal of Electronic Packaging*, Vol. 126, pp. 410-422.

9. Phillips, R.J., (1990), "Microchannel Heat Sinks", *ASME Advances in Thermal Modeling of Electronic Components and Systems*, Vol. 2, pp. 109-184.

10. Knight, R.W., Hall, D.J., Goodling, J.S. and Jaeger, R.C., (1992), “Heat sink optimization with application to microchannels”, *IEEE Transactions on Components, Hybrids and Manufacturing Technology*, Vol. 15, pp. 832-842.

11. Weisberg, A. and Bau, H.H., (1992), “Analysis of microchannels for integrated cooling”, *International Journal of Heat and Mass Transfer*, Vol. 35, pp. 2465-2474.

12. Yin, X. and Bau, H.H., (1997), “Uniform channel micro heat exchangers”, *Journal of Electronic Packaging*, Vol. 119, pp. 89-95.

13. Fedorov, A.G. and Viskanta, R., (2000), “Three-dimensional conjugate heat Transfer in the microchannel heat sink for electronics packaging”, *International Journal of Heat and Mass Transfer*, Vol. 43, pp. 399-415.

14. Harpole, G.M. and Eninger, J.E., (1991), “Microchannel heat exchanger optimization”, *IEEE Proceedings of the Seventh Semi-Therm Symposium*, Vol. 361, pp, 59-63.

15. Copeland, D., Behnia, D. and Nakayama, W., (1996), “Manifold microchannel heat sinks: Isothermal analysis”, *IEEE Proceedings of the Fifth Intersociety Conference on Thermal Phenomena in Electronic Systems*, pp. 251-257.

16. Ng, E.Y.K. and Poh, S.T., (1999), “Investigative study of manifold microchannel heat sinks for electronic cooling design”, *Journal of Electronics Manufacturing*, Vol. 9, pp. 155-166.

17. Hung, T.C., Wangi S.K. and Tsai, F.P., (1997), “Simulation of passively enhanced conjugate heat transfer across an array of volumetric heat sources”, *International Journal for Numerical Methods in Engineering*, Vol. 13, pp. 855-866.

18. Li, J., Peterson, G.P. and Cheng, P., (2004), “Three-dimensional analysis of heat Transfer in a micro-heat sink with single phase flow”, *International Journal of Heat and Mass Transfer*, Vol. 47, pp. 4215-4231.

19. Masud, Bebnia,, Wataru, Nakayama. and Jeffrey, Wan., (1998), “CFD simulations of heat transfer from a heated module in an air Stream: comparison with experiments and a parametric study”, *IEEE Intersociety Conference on Thermal Phenomena*, Vol. 54, pp. 539-544.

20. Dhiman, A.K., Chhabra, R.P. and Eswaran, V., (2005), "Flow and heat transfer across a confined square cylinder in the steady flow regime: effect of peclet number", *International Journal of Heat and Mass Transfer*, Vol. 48, pp. 4598-4614.

21. Cheng, Y.P., Lee, T.S. and Low, H.T., (2006), "Numerical analysis of mixed convection in three-dimensional rectangular channel with flush mounted heat sources based on field synergy principle", *International Journal for Numerical Methods in Fluids*, Vol. 52, pp. 987-1003.

22. Kumara, K.S., Tulapurkaraa, E.G., Biswasb, G. and Gowdac, B.H.L., (2005), "Reverse flow in channel with obstruction at entry", *Fluid Dynamic Research*, Vol. 37, pp. 387-398.

23. Roy, A. and Bandyopadhyay, G., (2004), "Numerical investigation of confined flow past a square cylinder placed in a channel", *Journal of Institution of Engineers*, Vol. 85, pp. 60-63.

24. Rodgers, P.J., Eveloy, V.C. and Davies, M.R.D., (2003), "An experimental assessment of numerical predictive accuracy for electronic component heat transfer in forced convection", *ASME Journal of Electronic Packaging*, Vol. 125, pp. 76-83.

25. Qu, W. and Mudawar, I., (2002), "Analysis of three-dimensional heat transfer in microchannel heat sinks", *International Journal of Heat and Mass Transfer*, Vol. 45, pp. 3973-3985.

26. Ryu, J.H., Choi, D.H. and Kim, S.J., (2003), "Three-dimensional numerical optimization of a manifold microchannel heat sink", *International Journal of Heat and Mass Transfer*, Vol. 46, pp. 1553-1562.

27. Vafai, K. and Zhu, Lu., (1999), "Analysis of two-layered microchannel heat sink concept in electronic cooling", *International Journal of Heat and Mass Transfer*, Vol. 42, pp. 2287-2297.

28. Pfund, D., Rector, D., Shekarriz, A., Popescu, A. and Welty, J., (2000), "Pressure drop measurements in a microchannel", *International Journal of Heat and Mass transfer*, Vol. 46, pp. 1496-1507.

29. Tuckerman, D.B. and Pease, R.F., (1981), "High performance heat sinking for VLSI", *IEEE Electronic Devices Letters*, Vol. 2, pp. 126-129.

30. Wong, H. and Peck, R.E., (2001), “Experimental evaluation of air-cooling electronics at high altitudes”, *ASME Journal of Electronic Packaging*, Vol. 123, pp. 356-365.

31. Haider, S.I., Joshi, Y., Nakayama, K. and Wataru., (2002), “A natural circulation model of the closed loop two phase thermosyphon for electronics cooling”, *ASME Journal of Heat Transfer*, Vol. 124, pp. 881-890.

32. Yoo, Seng-Yeon., Park, Jong-Heon. and Chung, Min-Ho., (2003), “Local heat transfer character in simulated electronic modules”, *ASME Journal of Electronic Packaging*, Vol. 125, pp. 362-368.

33. Rhee, Jinny., Moffat. and Robert J., (2006), “Experimental estimate of the continuous one-dimensional kernel function in a rectangular duct with forced convection”, *ASME Journal of Heat Transfer*, Vol. 128, pp. 811-818.

34. DeVoe, Jason. and Ortega, Alfonso., (2000), “An investigation of board level effects on compact thermal models of electronics chip packages”, *IEEE SEMI-THERM Symposium*, Vol. 24, pp. 191-198.

35. Pfahler, J., Harley, J., Bau, H.H. and Zemel, J., (1991), “Gas and liquid flow in small channels”, *ASME Micromechanical Sensors, Actuators and Systems*, Vol. 32, pp. 49-60.

36. Peng, X.F. and Peterson, G.P., (1996), “Concective heat transfer and flow friction for water flow in microchannel structures”, *Intenational Journal of Heat and Mass Transfer*, Vol. 39, pp. 2599-2608.

37. Peng, X.F. and Wang, B.X., (1994), “Experimental investigation on forced flow convection heat transfer through microchannels”, *Intenational Journal of Heat and Mass Transfer*, Vol. 37, pp. 73-82.

38. Papautsky, I., Brazzle, J., Ammel, T. and Frazier, A.B., (1999), “Laminar fluid behavior in microchannels using micropolar fluid theory”, *ASME Micromechanical Sensors and Actuators*, Vol. 73, pp. 101-108.

39. Mala, G.M. and Li, D., (1999), “Flow characteristics of water in microtubes”, *International Journal of Heat and Fluid Flow*, Vol. 20, pp. 142-148.

40. Mala, G.M., Li, D., Werner C., Jacobasch, H.J. and Ning, Y.B., (1997), “Flow characteristics of water through microchannels between two parallel plates with

electrokinetic effects", *International Journal of Heat and Fluid Flow*, Vol.18, pp. 489-496.

41. Tso, C.P. and Mhullikar, S.P., (1998), "The use of the brinkman number for single phase forced convective heat transfer in microchannels", *International Journal of Heat and Mass Transfer*, Vol. 41, pp. 1759-1769.

42. Xu, B., Ooti, K.T. and Wong, N.T., (2000), "Experimental investigation of flow friction for liquid flow in microchannels", *International Communications in Heat and Mass Transfer*, Vol. 27, pp. 1165-1176.

43. Liu, D. and Garimella, S.V., (2002), "Investigation of liqiud flow in microchannels", *Eighth AIAA/ASME Joint Thermophysis and Heat Transfer Conference*, St. Loius, Missouri, Vol. 5, pp. 2002-2776.

44. Lee, P. and Garimella, S.V., (2003), "Experimental investigation of heat transfer in microchannels", Paper No. HT2003-47293, *ASME Proceedings of HT2003 Summer Heat Transfer Conference*, Vol. 37.

45. Baviere, R., Ayela, F., Person, S.Le. and Favre-Marinet, M., (2004), "An experimental study of water flow in smooth and rough rectangular microchannels", *Second International Conference on Microchannels and Minichannels*, Rochester, New York, Vol. 25, pp. 221-228.

46. Harms, T.M., Kazmierczak, M.J. and Gerner, F.M., (1999), "Developing convective heat transfer in deep rectangular microchannels", *ASME International Journal of Heat and Fluid Flow*, Vol. 20, pp. 149-157.

47. Choi, S.B., Barron, R.F. and Warrington, R.O., (1991), "Fluid flow and heat transfer in microtubes", *ASME Micromechanical Sensors, Actuators, and Systems*, Vol. 32, pp. 123-134.

48. Rahman, M.M. and Gui, F., (1993), "Experimental measurements of fluid flow and heat transfer in microchannel cooling passages in a chip substrate", *ASME International Electronics Packaging Conference*, Binghamton, New York, USA, Vol. 4, pp. 685-692.

49. Rahman, M.M. and Gui, F., (1993), "Design, fabrication and testing of microchannel heat sinks for aircraft avionics cooling", *Proceedings of the Intersociety Energy Conversion Engineering Conference*, Vol. 1, pp. 1-6.

50. Jung, J.Y. and Kwak, H.Y., (2008), "Fluid flow and heat transfer in microchannels with rectangular cross-section", *Heat and Mass Transfer*, Vol. 44, pp. 104-1049.

51. Lee, P.S., Garimella, S.V. and Liu, D., (2005), "Investigation of heat transfer in rectangular microchannels", *International Journal of Heat and Mass Transfer*, Vol. 48, pp. 1688-1704.

52. Adams, T.M., Abdel-Khalik, S.I., Jeter, S.M. and Qureshi, Z.H., (1998), "An experimental investigation of single-phase forced convection in microchannels", *International Journal of Heat and Mass Transfer*, Vol. 41, pp. 851-857.

53. Celata, G.P., Cumo, M., Guglielmi, M. and Zummo, G., (2002), "Experimental investigation of hydraulic and single-phase heat transfer in 0.130 mm capillary tube", *Microscale Thermophysical Engineering*, Vol. 6, pp. 85-97.

54. Bucca, A., Celata, G.P., Cumo, M., Serra, E., and Zummo, G., (2003), "Water single-phase fluid flow and heat transfer in capillary tubes", *Procedings of the First International Conference on Microchannels and Minichannels*, Rochester, New York, Vol. 7, pp. 24-25.

55. Harms, T.M., Kazmierczak, M.J. and Gerner, F.M., (1999), "Developing convective Heat transfer in deep rectangular microchannels", *International Journal of Heat and Fluid Flow*, Vol. 20, pp. 149-157.

56. Qu, W. and Mudawar, I., (2002), "Experimental and numerical study of pressure drop and heat Transfer in a single-phase microchannel heat sink", *International Journal of Heat and Mass Transfer*, Vol. 45, pp. 2549-2565.

57. Owhaib, W. and Palm, B., (2004), "Experimental investigation of single-phase convective heat transfer in circular microchannels", *Experimental Thermal and Fluid Science*, Vol. 28, pp. 105-110.

58. Kohl, M.J., Abdel-Khalik, S.I., Jeter, S.M. and Sadowski, D.L., (2005), "An experimental investigation of microchannel flow with internal pressure measurements", *International Journal of Heat and Mass Transfer*, Vol. 48, pp. 1518-1533.

59. Zeighami, R., Laser, D., Zhou, P., Asheghi, M., Devasenathipathy, S., Kenny, T., Santiago, J. and Goodson, K., (2000), "Experimental investigation of flow transition in microchannels using micro-resolution particle image velocimetry", *Proceedings of the*

Intersociety Conference, Vol. 2, pp. 148-153.

60. Guo, Z.Y. and Li, Z.X., (2003), "Size effect on microscale single-phase flow and heat transfer", *International Journal of Heat and Mass Transfer*, Vol. 46, pp. 149-159.

61. Lee, S.Y., Wereley, S.T., Gui, L., Qu, W. and Mudawar, I., (2002), "Microchannel flow measurement using micro particle image velocimetry", *American Society of Mechanical Engineers Fluids Engineering Division*, Vol. 258, pp. 493-500.

62. Tu, X. and Hrnjak, P., (2003), "Experimental investigation of single-phase flow pressure drop through rectangular microchannels", *ASME International Conference on Microchannels and Minichannels,* Vol. 1, pp. 257-267.

63. Sharp, K.V. and Adrian, R.J., (2004), "Transition from laminar to turbulent flow in liquid filled microtubes", *Experiments in Fluids*, Vol. 36, pp. 741-747.

64. Lior, H., Ewoldt, R., and Olsen, M.G., (2005), "Turbulent and transitional velocity measurements in a rectangular microchannel using microscopic particle image velocimetry", *Experimental Thermal and Fluid Science*, Vol. 29, pp. 435-446.

65. Li, H and Olsen, M.G., (2006), "Aspect ratio effects on turbulent and transitional flow in rectangular microchannels as measured with micro PIV", *Journal of Fluids Engineering*, Vol. 128, pp. 305-315.

66. Li, H. and Olsen, M., (2006), "Micro PIV measurements of turbulent flow in square microchannels with hydraulic diameters from 200 m to 640 m", *International Journal of Heat and Fluid Flow*, Vol. 27, pp. 123-134.

67. Steinke, M. and Kandlikar, S.G., (2006), "Single-phase liquid friction factors in microchannels", *International Journal of Thermal Sciences*, Vol. 45, pp. 1073-1083.

68. Judy, J., Maynes, D. and Webb, B.W., (2002), "Characterization of frictional pressure drop for liquid flows through microchannels", *International Journal of Heat and Mass Transfer*, Vol. 45, pp. 3477-3489.

69. Kawano, K., Minakami, K., Iwasaki, H. and Ishizuka, M., (1998), "Development of microchannels heat exchanging", in: Nelson Jr, R.A., Swanson, L.W., Bianchi, M.V.A., Camci, C. (Eds.), *ASME Application of Heat Transfer in Equipment, Systems and Education*, Vol. 361, pp. 173-180.

70. Pak, B.C., Copeland, D. and Nakayama, W., (1995), “Cooling of electronic systems by using manifold microchannel heat sinks”, *Proceedings of KSME Fall Annual Meeting*, Korea, Vol. 2, pp. 74-80.

71. Kim, Y.I., Chun, W.C., Kim, J.T., Pak, B.C. and Back, B.J., (1998), “Forced air cooling by using manifold microchannel heat sinks”, *KSME International Journal*, Vol. 12, pp. 709-718.

72. Tae hoji, Z.Y. and Li, Z.X., 2003, “Size effect on microscale single-phase flow and heat transfer”, *International Journal of Heat and Mass Transfer*, Vol. 46, pp. 149-159.

73. Wu, P. and Little, W.A., (1983), “Measurement of friction factors for the flow of gasses in very fine channels used for microminiature joule-thompson refrigerators, cryogenics”, *Journal of Thermal Science and Technology*, Vol. 23, pp. 273-277.

74. Bejan, A., (1984), “Convective heat transfer”, first ed., New York.

75. FLUENT Inc, (1998), “Fluent User’s Guide”, Lebanon, New Hampshire.

CFD ANALYSIS ON FORCED CONVECTION COOLING OF ELECTRONIC CHIPS

A THESIS SUBMITTED IN PARTIAL FULFILMENT
OF THE REQUIREMENTS FOR THE DEGREE OF

ADDENDUM

Master of Technology (Research)

in

Mechanical Engineering

by

SHAKUNTALA OJHA

Department of Mechanical Engineering
National Institute of Technology
Rourkela
2009

ADDENDUM

I Shakuntala Ojha M.Tech (Res) in Mechanical Engineering, with specialization in "Thermal Engg." at National Institute of Technology, Rourkela (Deemed University) submit these clarifications as addenda of my thesis "**CFD ANALYSIS ON FORCED CONVECTION COOLING OF ELECTRONIC CHIPS**".

Shakuntala Ojha

Date: - **Roll No: - 60703001**

National Institute of Technology

Rourkela-769008, Orissa, India

General comments to be addressed

1. Regarding the organization of the thesis: *Section 1.6*, '*Background of Theory*': Instead "*Theoretical Background*" may be appropriate. Slip flow, Knudsen number, thermal accommodation coefficient,.. How they are related to the present research work? A discussion regarding the legacy of those concepts to the developed model, and the assumption taken, in precise, towards the model development is pertinent. There exists slip flow even for liquid flow through microchanels, hence the definition of slip flow need modification. 'CMOS' used in *Section 1.3.2.4* is not induced in abbreviation list.

   Section 1.6,' *Background of Theory*'

   For Navier Stokes Equations with no slip boundary condition Kn should be less than 10^{-3}.

$$Kn = \frac{\lambda}{L}$$

$$= \frac{2.56 \times 10^{-8}}{86.58 \times 10^{-6}} = 2.95 \times 10^{-4}$$

   Since it was obeying the range of $Kn < 10^{-3}$, the fluid can be treated as continuous medium.

   For water as working fluid, the effect of slip flow, thermal accommodation coefficient are assumed to be negligible.

   If air as working medium:

$$Kn = \frac{\lambda}{L}$$

$$= \frac{8 \times 10^{-8}}{86.58 \times 10^{-6}} = 9.24 \times 10^{-4}$$

Source: M. H. C. Knudsen; Denmark [1871-1949] rheology. Symbol Kn. Relating to momentum transport in rarefied gases, the dimensionless ratio of the mean free path of the molecules to a representative length. International Standards Association

   Section 1.3.2.4

   CMOS: - Complementary Metal oxide Semiconductor.

2. In which ways does the present work can be considered to be different and incremental research work so far as the work of Li et. al. (18) is concerned?

In Li et.*al.* [18],

i. A finite difference numerical code was developed using a Tri-Diagonal Matrix Algorithm to solve the governing equation.

ii. The geometric parameters of the channel and the thermophysical properties of the fluid on the flow and the heat transfer, are investigated using a temperature dependent. thermophysical property method.

But in the present research work,

i. A three dimensional CFD model was built using the commercial package, FLUENT, to investigate the conjugate fluid flow and heat transfer phenomena in a silicon based rectangular microchannel heat sink.

ii. The geometric parameter of the channel and the thermophysical properties of the fluid flow and the heat transfer are investigated using a temperature independent.

3. The used parameters like S_b and S_t in *chapter 3* is neither induced explicity in the nomenclature section nor those have in explained after *Table 3.1*. *Section 3.4*: "the simulation strats from the heat flux boundary with ***gravity along y direction***' the gravity is not along y direction but along (-y) direction. In Y-momentum equation no body force is induced? If the eqs. (3.2) & (3.4). it has been stated in *Section 3.5* that "compressibility, viscous dissipation (heat), and the **gravitational force have been neglected**…" . actually gravitation is neglected along (–y) direction. *Section 3.4* and *3.5* are to be in harmony and perfectly synchronized with lucidity.

In chapter 3

S_b :- Height from bottom of the substrate to the bottom of the microchannel.

S_t :- Height from the top of the heat sink to the top of the channel.

The simulation starts from the heat flux boundary along *y*-direction. Here the analysis is about forced convection, so the effect of gravity is neglected.

Body force such as gravity, centrifugal, surface tension is neglected. So in Y-momentum equation no body force is induced.

In equation 3.3 the pressure is hydrostatic pressure. Since the flow is an internal flow, the

flow is pressure driven. $\frac{\partial p}{\partial x}$ pressure gradient which is responsible to cause the flow.

In section 3.5 that compressibility, viscous dissipation and the gravitational force have been neglected. Here the effect of gravity along y-direction has been neglected.

4. Grid independence test: how many sets were done? The grid density used for every combination? What criterion was chosen to specify optimum grid combination as 10(x) × 100(y) × 200(z)? for that one has to compare certain predictions (simulated result) for different sets of grid combinations.

   In section 4.2.1

   The model in this study uses a total number of grid 2,00000 (i (x)× j (y) × k (z) = 10 × 100 × 200). Here only one case has given but it is done for all combination of heat flux, pressure. The grid density used for every combination. Due to machine limitation, one cannot take more mesh in *Z*-direction.

   Convergence criterion

   Continuity - 0.001

   X - velocity = 0.001

   Y - velocity = 0.001

   Z - velocity= 0.001

   Energy= 1e-06

   In the present configuration the above criterion is found to be optimum for the convergence of the solution.

5. *In section 4.2.2*: it has been stated the model proposed in the present study yields a better agreement in average heat transfer coefficient with numerical results? Which were the numerical results used for the comparison?

   In section 4.2.2

   For better agreement the average Nusselt number result have been compared with Li's numerical result which was shown in Fig. 4.1.

6. *In section 4.3.4*: h_{av} was calculated cell wise along z direction? How the wall temperature and bulk fluid temperature were considered? They were not stated clearly.

In section 4.3.4

The average heat transfer coefficient has been calculated by taking four points at top, bottom and side wall at a distance (x ,y)= (0.005, 0.000179), (0.005, -0.000179), (-0.005, -0.000179) and (-0.005, 0.000179) along channel length. Then at each grid point FLUENT has calculated the value of heat transfer coefficient. Then adding all the values the average value of heat transfer coefficient is calculated. The average wall temperature and the bulk fluid temperature were calculated directly by FLUENT.

In section 4.3.5 what was the definition used for average Nusselt number in different *x-y* plane along z direction? The first two lines of this section do not convey the context and meaning correctly. Anyway, these kinds of grammatical style and language modification could be taken into account throughout the organization of the thesis.

In section 4.3.5

The average Nusselt number is defined as follows

$$Nu_{avg} = \frac{h_{avg} . D_h}{k_f}$$

Where h_{avg} = average heat transfer coefficient

D_h = hydraulic diameter

k_f = thermal conductivity of fluid

7. Is there any relevance to determine h_{av} as well as Nusselt number for the liquid flow through microchannel of the specified dimension?

It is relevant to calculate average heat transfer coefficient and Nusselt number for 3-Dimensiomal flow.

8. *In section 4.3.8*: how the average heat flux was defined at the top, bottom or side wall of x-y plane? It was not clearly stated.

Adiabatic boundary conditions are applied to all the boundaries of solid region ie top and

side wall of heat sink except the bottom wall, where a constant heat flux is applied. The average heat flux was calculated by FLUENT in y-direction along channel length at all the walls except bottom wall of heat sink.

9. Literature citations until 2006 were present but nothing were cited from 2007 and onwards?

1. Hong, F.J; Cheng, P; Ge, H and Goh, Teck Joo, 2007, "Conjugate heat transfer in fractal shaped Microchannel network heatsink for integrated microelectronicg cooling application", *International Journal of Mass and Heat Transfer*, pp. 4986-4998.
2. Wang, G.D; Cheng, P andWu, Huiying, 2007, " Unstable and stable flow boiling in parallel microchannel and in a single microchannel", *Journal of Heat Transfer*.
3. Agostini, B; Thome, R.j; Fabbri, M; Michel, B; Calmi, D and Kloter, U, 2008, "High heat flux boiling in silicon multi channel Part 1: Heat transfer characterstics of refrigerant R 236fa", *Journal of Heat Transfer*.
4. Agostini, B; Thome, R.j; Fabbri, M; Michel, B; Calmi, D and Kloter, U, 2008, "High heat flux boiling in silicon multi channel Part 1: Heat transfer characterstics of refrigerant R 245fa", *Journal of Heat Transfer*.
5. Garmat,G; Favre-Marinet, M; Person, S.Le and Cheng, P, 2009, "Modelingof roughness effecs on heat transfer in thermally fully developed laminar flow through microchannel", *International Journal of Heat Mass Transfer*.
6. Mokrani, Om; Baurouga, Br; Castelain, Ca and Peerhossaini, Ha, 2009, "Fluid flow andconvective heat transfer in flat microchannel", *Journal of Heat Transfer*.

The hydrodynamic and thermal characteristics of fractal shaped microchannel network heat sinks are investigated numerically [1] by solving three-dimensional N-S equations and energy equations, taking in to consideration of the conjugate heat transfer in microchannel walls. It is found that due to the structural limitation of right angled fractal shaped microchannel network, hotspot may appear on the bottom wall of the heat sink where the microchannels are sparsely distributed.

A simultaneous visualization and measurement study have been carried out [2] to investigate flow boiling instabilities of water in microchannels at various heat fluxes and mass fluxes. Two separate flow boiling experiments were conducted in eight parallel silicon microchannels (with flow interaction from neighboring channels at headers) and in a single microchannel (without flow interaction), respectively. These microchannels, at a length of 30 mm, had an identical trapezoidal cross-section with a hydraulic diameter of 186 μm. At a given heat flux and inlet water temperature, it was found that stable and unstable flow boiling regimes existed, depending on the mass flux. A flow boiling map, in terms of heat flux vs mass flux, showing stable flow boiling regime and unstable flow boiling regime is presented for parallel microchannels as well as for a single microchannel, respectively, at an inlet water temperature of 35^{o}C.

This article [3] is the first in a three part study on flow boiling of refrigerants R236fa and R245fa in a silicon multi-microchannel heat sink. The heat sink was composed of 67 parallel channels, which are 223 μm wide, 680 μm high and 20 mm long with 80 μm thick fins separating the channels. The base heat flux was varied from 3.6 to 221 W/cm^2,
the mass velocity from 281 to 1501 kg/m^{2}s and the exit vapor quality from 2% to 75%. The working pressure and saturation temperature were set nominally at 273 kPa and 25^{o}C, respectively. The present database includes 1217 local heat transfer coefficient measurements, for which three different heat transfer trends were identified, but in most cases the heat transfer coefficient increased with heat flux and was almost independent of vapor quality and mass velocity. Importantly, it was found for apparently the first time that the heat transfer coefficient as a function of vapor quality reaches a maximum at very high heat fluxes and then decreases with further increase of heat flux.

This article [4] is the second in a three-part study. This second part focuses on flow boiling heat transfer of refrigerant R245fa in a silicon multi-microchannel heat sink and their comparison with the results presented in part I for refrigerant R236fa. This heat sink was the same as utilized in part I. The test conditions covered base heat fluxes from 3.6 to 190 W/cm^2, mass velocities from 281 to 1501 kg/ m^{2}s and the exit vapor qualities from 0% to 78%. The effect of saturation pressure on heat transfer was tested from 141 to 273 kPa for R245fa and the effect of sub-cooling from 0 to 19 K. The R245fa database

includes 693 local heat transfer coefficient measurements, for which four different heat transfer trends were identified, although in most cases the heat transfer coefficient increased with heat flux, was almost independent of vapor quality and increased with mass velocity.

In this paper [5], roughness was modeled as a pattern of parallelepiped elements of height k periodically distributed on the plane walls of a microchannel of height H and of infinite span. Two different approaches were used to predict the influence of roughness on heat transfer in laminar flows through this microchannel. Three-dimensional numerical simulations were conducted in a computational domain based on the wave length . A one- dimensional model (RLM model) was also developed on the basis of a discrete-element approach and the volume averaging technique. The numerical simulations and the rough- layer model agree to show that the Poiseuille number Po and the Nusselt number Nu increase with the relative roughness. The RLM model shows that the roughness effect may be interpreted by using effective roughness heights keff and keffq for predicting Po and Nu respectively. The present results show that roughness increases the friction factor more than the heat transfer coefficient (performance evaluation criteria < 1), for a relative roughness height expected in the fabrication of microchannels ($k/(H/2) < 0.46$) or $k/Dh < 0.11$).

This study [6] investigates the design, construction and instrumentation of an experimental microchannel, with a rectangular cross-section and large aspect ratio, that allows characterization of the flow and convective heat transfer under well defined and precise conditions and makes it possible to vary the hydraulic diameter of the microchannel. The flow friction coefficient is estimated by direct pressure drop measurements inside the microchannel in a zone where the flow is fully developed. Since the wall thermal conditions inside the microchannel can not be measured directly, their estimation requires temperature measurements in the wall thickness and an inverse heat conduction method. The thermal and hydrodynamic results obtained by varying the hydraulic diameter between 1 mm and 100 μm do not deviate from the theory or empirical correlations for large-scale channels. These results let us confirm that for smooth walls the continuum mechanics laws for convection and fluid mechanics remain valid in microchannels of hydraulic diameter greater than or equal to 100 μm.

Comments to be Addressed Specifically

1. In the present work no-slip boundary condition was assumed in a microchannel flow of channel dimension 10mm×57μm×180μm.in this microchannel dimension continuum is not broken but there remains a possibility of slip flow over rough or smooth walls(Experimental evidences are there in G. Karniadais, A. Beskok, N. Aluru (2004).Microflow and nano flow fundamentals and simulation, Springer, Los Angeles, CA; Kundu et al.(2009), Asia-pac.J.Chem Engg,4:450-461). The slip flow model can be of Maxwell's slip flow model utilizing molecular mean free path concept or a slio flow over a practically feasible slip length.

   It should be checked a priori, whether a no-slip boundary condition is applicable at all, by calculating the Knudsen number and seeing whether the physical dimensions of the fluid demands for the slip flow analysis?

   The global Knudsen number (Kn_g) in the present microchannel flow is to be determined first. The determined Knudsen number then dictates' whether the flow is in continuum regime (Kn_g<0.001, Nivier-Stokes equation with slip flow boundary condition governs the flow) or it is in slip flow regime (0.01≤ Kn_g≤0.1, Nivier-Stokes equation with slip flow and temperature jump boundary conditions govern the flow). The assumption of negligible viscous dissipation can also be addressed on the basis of slip boundary condition.

   In micro fluid, the knowledge of liquid flow is less explored and developed than gas flow. In view of this, justifying the use of no-slip and no temperature jump conditions in the present work on the basis of determined Kn_g),Even for liquid flow through the microchannel heat sink) might not be appropriate here.

   As already discussed about slip flow, Knudsen number and thermal accommodation coefficient in *section 1.6*

2. What is the maximum Reynold's attained in the microchannel flow? Is it 105? Does the Re value is in accordance with the laminar flow assumption?

$$Re = \frac{\rho v D_h}{\mu}$$

$$= \frac{998.2 \times 1.22 \times 86.58 \times 10^{-6}}{0.001003} = 105$$

Minimum *Re*=105 for hydrostatic pressure 50000 Pascal at velocity 1.22m

Maximum *Re*= 336.04 for hydrostatic pressure 50000 Pascal at velocity 3.9m